© 2022. Published by The Company of Biologists Ltd | Journal of Cell Science (2022) 135, jcs259513. doi:10.1242/jcs.259513

RESEARCH ARTICLE

Unveiling a novel serpinB2-tripeptidyl peptidase II signaling axis during senescence

Chia-Li Liao[1,*], Rong-Chi Hu[1,*], Min-Shiang Liao[2,*], Yi-Ju Chen[3], Ya-Ping Chen[2], Hsi-Hsien Hsieh[4], Chih-Hsuan Tai[2], Tzyy-Chao Chou[2], Chi-Yuan Chu[2], Yu-Ju Chen[3], Lee-Chiang Lo[2,‡] and Jing-Jer Lin[1,‡]

ABSTRACT

Tripeptidyl peptidase II (TPPII or TPP2) degrades N-terminal tripeptides from proteins and peptides. Studies in both humans and mice have shown that TPPII deficiency is linked to cellular immune-senescence, lifespan regulation and the aging process. However, the mechanism of how TPPII participates in these processes is less clear. In this study, we established a chemical probe-based assay and found that although the mRNA and protein levels of TPPII were not altered during senescence, its enzymatic activity was reduced in senescent human fibroblasts. We also showed that elevation of the levels of the serine protease inhibitor serpinB2 reduced TPPII activity in senescent cells. Moreover, suppression of TPPII led to elevation in the amount of lysosomal contents as in well as TPPI (TPP1) and β-galactosidase activities, suggesting that lysosome biogenesis is induced to compensate for the reduction of TPPII activity in senescent cells. Together, this study discloses a critical role of the serpinB2-TPPII signaling pathway in proteostasis during senescence. Since serpinB2 levels can be increased by a variety of cellular stresses, reduction of TPPII activity through activation of serpinB2 might represent a common pathway for cells to respond to different stress conditions.

This article has an associated First Person interview with the first author of the paper.

KEY WORDS: Activity-based probe, Serine hydrolase, TPP, Senescence, Benzylphosphonofluoridate

INTRODUCTION

Tripeptidyl peptidases (TPPs) are enzymes that degrade N-terminal tripeptides from oligopeptides generated by other proteases (Tomkinson, 1999). Two types of tripeptidyl peptidases, TPPI and TPPII (also known as TPP1 and TPP2, respectively), exist in eukaryotic cells. TPPI is a lysosomal acidic protease, responsible mainly for lysosomal protein degradation. A notable case of TPPI dysfunction in humans is its association with a lysosomal storage disease called neuronal ceroid lipofuscinosis (NCL). In particular, mutations in TPPI develop a classical late-infantile NCL, an inherited neurodegenerative disorder of childhood (Cárcel-Trullols et al., 2015). Although the detailed mechanisms are unknown, TPPI might also have a role in macro-autophagy, endocytosis and TNF-α (also known as TNF)-induced apoptosis (Autefage et al., 2009; Micsenyi et al., 2013; Vidal-Donet et al., 2013). TPPII, on the other hand, is a cytosolic protease that is known to function downstream of the proteasome-ubiquitin pathway for protein degradation (Tomkinson, 1999). It forms a large oligomeric complex (~5–6 MDa) with a spindle-like shape (Rockel et al., 2012). Because TPPII levels are high in immune cells (Balow et al., 1986; Huai et al., 2008), mutations in TPPII have been shown to selectively affect immune system by impairing the function of adaptive and innate immunity (Huai et al., 2008; Stepensky et al., 2014). As a result, deficiency of TPPII is linked to autoimmune cytopenia in Evans syndrome, which shows severe immune deficiencies (Stepensky et al., 2014). In addition to cellular immune senescence, analyses of the *Tpp2*$^{-/-}$ knockout cells and mice also suggest that TPPII is involved in several vital cellular processes, such as cell proliferation and survival, and in diseases such as muscle wasting, obesity and cancer (Huai et al., 2008; Rockel et al., 2012; Tomkinson, 1999). In another example, TPPII contributes to the survival of Burkett's lymphoma (BL) cells that had been treated with proteasome inhibitors (Gavioli et al., 2001). These results suggest that TPPII is upregulated in response to the loss of the proteasome degradation pathway in BL cells.

Normal human diploid fibroblasts enter the terminally non-dividing state after ~60–80 population doublings (PDs). This limited proliferative capacity of normal fibroblasts is termed replicative senescence or cellular senescence (Hayflick, 1965; Hayflick and Moorhead, 1961). Cellular senescence is caused by progressive telomere shortening after repeated cycles of cell divisions (Allsopp et al., 1995; Bodnar et al., 1998). Senescence can also be induced by a variety of factors ranging from inadequate culturing conditions to overexpression of oncogenes (Serrano et al., 1997; Sherr and DePinho, 2000). This category of senescence, caused by cultural or mitotic shocks, is independent of telomere length. Nowadays, senescence is well recognized as a state of cell cycle arrest in response to various types of stress (Campisi and d'Adda di Fagagna, 2007). In addition to proliferation cessation, senescent cells show distinct morphological changes (Salama et al., 2014). Senescent cells usually become larger, flattened and vacuolized, and show increased lysosomal mass. The most widely used assay for senescence is the histochemical detection of β-galactosidase activity at pH 6.0, which is known as senescence-associated β-galactosidase (SA-β-gal) (Dimri et al., 1995). The increased levels of SA-β-gal are caused by the increased lysosomal content of senescent cells (Kurz et al., 2000; Lee et al., 2006). However, unlike cessation of cell proliferation, the mechanisms underlying diverse phenotypic alterations of senescent cells remain less clear. The involvement of TPPII in senescence has been previously inferred by using genetic inactivation of TPPII. It was found in both human and mice that depletion of TPPII is sufficient

[1]Institute of Biochemistry and Molecular Biology, National Taiwan University College of Medicine, Taipei 100, Taiwan. [2]Department of Chemistry, National Taiwan University, Taipei 106, Taiwan. [3]Institute of Chemistry, Academia Sinica, Taipei 115, Taiwan. [4]Institute of Biopharmaceutical Sciences, National Yang-Ming University, Taipei 112, Taiwan.
*These authors contributed equally to this work

‡Authors for correspondence (jingjerlin@ntu.edu.tw; lclo@ntu.edu.tw)

J.-J.L., 0000-0001-8250-7398

Handling Editor: John Heath
Received 25 October 2021; Accepted 15 April 2022

Journal of Cell Science (2022) 135, jcs259513. doi:10.1242/jcs.259513

to induce elevated levels of SA-β-gal activities in both immune cells and fibroblasts (Huai et al., 2008; Stepensky et al., 2014). Nevertheless, how TPPII participates in senescence and the mechanism of how TPPII-depleted cells induce senescence were not clear and demand further investigations.

In this study, we peculiarly observed that both the mRNA and protein levels of TPPII were not altered during senescence. This seemingly contradictory observation was puzzling. We therefore set out to establish a chemical probe-based activity assay to measure TPPII activity during senescence (Kuo et al., 2010). Interestingly, we found TPPII activity was decreased in senescent cells. We later found that suppression of TPPII activity was sufficient to induce senescence. More importantly, we found serine protease inhibitor serpinB2 interacts with TPPII and inhibited its activity. These critical results helped to reveal a novel signaling axis that depicts a post-translational regulation of TPPII activity by serpinB2 during senescence. We further demonstrate that inactivation of TPPII impairs proteostasis, leading to an increase in lysosome content as well as elevation of lysosomal TPPI and SA-β-gal activities. Since the serpinB2 level was also found to be elevated by different stresses in various cell types (Schroder et al., 2010; Zhang et al., 2015, 2009), results from this study further suggest that the serpinB2-TPPII signaling axis might be a pivotal mechanism for cellular stress response.

RESULTS

TPPII activity is suppressed in senescent cells

The normal human lung fibroblast line IMR90 was used as the model in this study. IMR90 cells were passaged continuously until the doubling rate became slow and they eventually stopped proliferating (Fig. 1A). The senescent cells are generally larger, less motile and have a lower saturation density. As shown in Fig. 1B, these cells also showed increased expression of SA-β-gal (Dimri et al., 1995). In this study, the cells at PD 5 and 20 were used to represent young and senescent cells, respectively. To test whether TPPII expression level was altered in senescent cells, the mRNA and protein levels of TPPII were determined by quantitative real-time RT-PCR (qRT-PCR) (Fig. 1C) and immunoblotting (Fig. 1D), respectively. It was to our surprise that the expression level of TPPII only fluctuated to a minor extent during senescence. This result seems to contradict previous reports suggesting that TPPII is involved in senescence.

Since proteases are strictly regulated to ensure their cellular functions, the possibility of alteration of TPPII activity in senescence was next investigated. To determine the protease activity of TPPII, here we applied a chemical probe-based assay protocol that has previously been exploited to measure designated protease, tyrosine phosphatase and kinase activities in proteomic samples (Chu et al., 2012; Hsu et al., 2016; Kuo et al., 2010; Sieber et al., 2004). A typical activity-based probe consists of a properly positioned reactive group, which is responsible for covalent bond formation with the target enzymes, and a reporter for visualization and/or purification of the covalently bound proteins. Here, we exploited probe **1** in this study (Fig. 1E). Probe **1** carries a benzylphosphonofluoridate as the reactive group and a biotin reporter group. It is anticipated that upon nucleophilic attack by the active site serine residue, the fluoride on probe **1** will depart and a stable biotinylated adduct will be formed.

To test the labeling property of probe **1**, the labeling reaction was first evaluated using trypsin (a serine protease) as a model. We found that probe **1** effectively labeled trypsin in an activity-dependent manner (Fig. 1F,G). The labeling reaction also appeared to be very robust as sub-micromolar concentrations of probe **1** was sufficient to label trypsin. Heat denatured or PMSF (a serine hydrolase inhibitor)-treated trypsin could not be labeled by probe **1**. The labeling reaction also appeared to be very robust as sub-micromolar concentrations of probe **1** was sufficient to label trypsin (Fig. S1A). The labeling reaction was next evaluated on other family of proteases. probe **1** effectively labeled serine hydrolases including trypsin, chymotrypsin and elastase. By contrast, no labeling was detected on aspartic proteases (pepsin and rennin), cysteine proteases (papain and bromelain) and the metalloprotease thermolysin (Fig. S1B). Data also showed that probe **1** could effectively label other members of serine hydrolases including esterase, chymotrypsin and elastase. Irrelevant targets such as glucosidase, phosphorylase b, protein tyrosine phosphatase PTP1B, γ-globulin, RNase A, lysozyme and carbonic anhydrase were not labeled by probe **1** (data not shown). Together these results indicated that probe **1** is a selective activity-based probe for serine hydrolases. More importantly, the labeling intensity reflects the enzymatic activity.

To enable the activity measurement of TPPII, we established an assay protocol that combines the use of probe **1** with a target specific antibody (Chu et al., 2012; Hsu et al., 2016; Kuo et al., 2010; Sieber et al., 2004). In this assay (Fig. 1H), the cell extracts were prepared and incubated with probe **1** to accomplish labeling of active serine hydrolases. After the labeling event, both forms of TPPII (labeled and unlabeled) were separated from the mixture through immunoprecipitation with a TPPII-specific antibody. Immunoblotting analyses were then conducted using antibodies against TPPII and biotin, respectively, to reveal the amounts of total TPPII and probe **1**-labeled TPPII. Using this assay protocol, we found the protein level of TPPII was not significantly altered, yet its activity was reduced during senescence (Fig. 1I). The results strongly imply that TPPII activity is suppressed in senescent cells by an unidentified inhibitor.

Probe **1** was also used to perform protein profiling during senescence. Total cell extracts were prepared from IMR90 cells at PD 5 and 20, and labeled with probe **1**. The probe **1**-labeled proteins were then enriched by streptavidin beads and subjected to mass spectrometry analysis. Comparative proteomic analysis of probe **1**-labeled proteins identified more than 20 serine hydrolases of which the activities were altered in senescent cells (Table S1). Consistent with the probe **1**-based activity assay, TPPII was identified as showing reduced activities in senescent cells. Taken together, our results indicate that the expression level of TPPII in senescent cells is not altered, yet the activity of TPPII is dramatically decreased.

Depletion of TPPII induces senescence phenotypes

To study the role of TPPII in senescence, we used shRNA to suppress the expression of the TPPII gene in normal fibroblasts. The TPPII levels were reduced in the shRNA-treated cells by 70% to 90% (Fig. 2A). The cellular effects of suppressing TPPII expression were then evaluated for these fibroblasts. The proliferation potential of the normal cells subjected to TPPII depletion was first examined. As shown in Fig. 2B, the number of TPPII-depleting cells did not increase after infection, indicating that TPPII-depletion inhibited proliferation of the cells. In addition, changes in the morphology of the TPPII-depleting fibroblasts were also observed. At 4 days after infection, the TPPII-depleting cells appeared to be flattened and enlarged, a phenotype similar to that of senescent cells (Fig. 2C). These results suggest that TPPII-depletion induces a senescence-like phenotype in normal fibroblasts. To confirm this observation, other senescence-associated features were also assessed in the TPPII-depleted fibroblasts. Senescence-associated β-galactosidase

Journal of Cell Science (2022) 135, jcs259513. doi:10.1242/jcs.259513

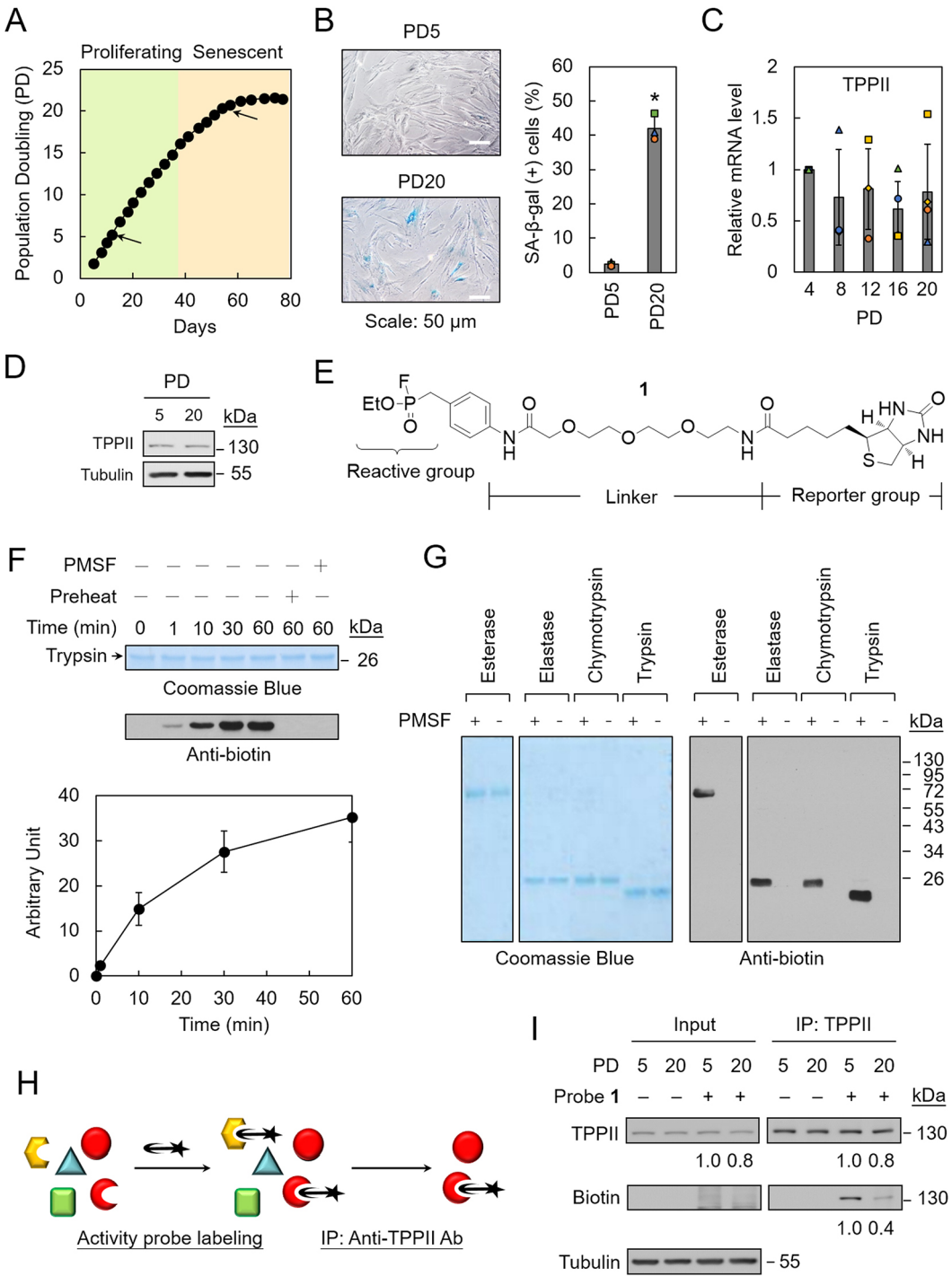

Fig. 1. See next page for legend.

(SA-β-gal) activity (Dimri et al., 1995) was therefore assessed in TPPII-depleted IMR90 cells. IMR90 cells with reduced TPPII levels showed an induction of SA-β-gal activity (Fig. 2C). The percentage of SA-β-gal-positive cells among GFP-only-expressing control cells was ∼5%. In contrast, over 20% of the TPPII-depleted cells stained positive for SA-β-gal activities. Consistent with this observation, the proportion of BrdU-incorporating cells (Wei and Sedivy, 1999) was also reduced from ∼38% for shLuc control cells to ∼20% for TPPII-depleted cells (Fig. 2D; Fig. S2).

It is known that senescent cells secrete immune modulators and inflammatory cytokines to reinforce senescence in an autocrine and paracrine manner (Sharpless and Sherr, 2015). The senescence-associated secretory phenotype (SASP) was thus analyzed in TPPII-depleted cells. We found the cellular senescence induced by TPPII-depletion also induced several signature SASP components, including interleukin (IL)6, IL8 and IL1α (Fig. 2E), suggesting that reduced TPPII level is sufficient to induce a secretory phenotype that is similar to senescence. Senescent cells also display a signature heterochromatin foci formation (Narita et al., 2003), which can be identified through elevated levels of histone 3 trimethylated at K9 (H3K9me3) or HP-1α. The TPPII-depleted cells were analyzed for formation of senescence-associated

Journal of Cell Science (2022) 135, jcs259513. doi:10.1242/jcs.259513

Fig. 1. TPPII activity is activated in senescent cells. (A) Population doublings (PDs) of IMR90 cells. Normal human lung fibroblasts IMR90 was continuously grown. After 20 PDs, the growth of IMR90 was slow and eventually cells stopped proliferating. Arrows indicated the proliferating cells at PD5 and senescent cells at PD20. Results representative of three repeats. (B) Senescence phenotype of IMR90 cells. The IMR90 cells at PD5 and PD20 were analyzed by SA-β-gal activity staining. Photographs of the X-gal-stained cells are shown (left). Quantification of the number of SA-β-gal-positive-stained cells was conducted (right). Results were obtained from the average of three independent experiments. **P*<0.05 (*P*=0.00003; paired two-tailed Student's *t*-test). (C) The mRNA levels of TPPII in young and senescent IMR90 cells. RNA from IMR90 cells with PD at 4, 8, 12, 16, and 20 were prepared and analyzed by qRT-PCR. GAPDH was used as an internal control and all samples were normalized to GAPDH. The values were obtained from the average of four independent experiments. Error bars represent s.d. (D) The protein levels of TPPI in young and senescent cells. Cell lysates prepared from IMR90 cells at PD5 (young) and PD20 (senescent) were separated by 10% SDS-PAGE and immunoblotted with antibody against TPPII or tubulin. (E) Structure of probe **1**. Probe **1** carries a benzylphosphonofluoridate and a biotin as the reactive and reporter group, respectively. (F) Efficient labeling of trypsin by probe **1**. 1 µg of trypsin was incubated with 1 µM probe **1** at 25°C for the indicated times and separated by 10% SDS-PAGE. The gels were stained with Coomassie Blue or subjected to immunoblotting analysis using anti-biotin antibody. Preheating of trypsin or addition of PMSF was used as a control. Quantification of the amount of labeled proteins was plotted (bottom panels). The values were obtained from the average of three independent experiments. Error bars represent s.d. (G) 1 µg of each of the indicated proteins was incubated with PMSF (1 mM) for 1 h. The treated protein was then incubated with probe **1** (3 µM) at 25°C for 10 min. (H) Schematic presentation of activity-based activity analysis of TPPII using probe **1**. The cell extracts are first incubated with probe **1** to label active TPPII. The probe **1**-labeled TPPII was immunoprecipitated (IP) by anti-TPPII antibody. The immunoprecipitated protein and activity of TPPII are determined by immunoblotted with anti-TPPII and biotin antibodies, respectively. (I) Immunoblots of experiment as in H. Input represents 10% of protein used for IP. Numbers below the blots represent normalized optical density of three independent experiments. Blot images in D, G and I are representative of three repeats.

heterochromatin foci (SAHF) by immunostaining using anti-HP1α antibody. As shown in Fig. S3, the TPPII-depleted cells did not display SAHF.

To gain insight into the molecular basis of TPPII-induced growth arrest and senescence in normal fibroblasts, the expression pattern of several key cell cycle regulators that are involved in senescence were examined using immunoblotting analysis. We found TPPII-depleting did not appear to induce p53 (also known as Tp53) expression. Although p21 and p16 (encoded by *Cdkn1a* and *Cdkn2a*, respectively) have been implicated as key mediators in senescence (Sharpless and Sherr, 2015), the levels of these two proteins were not altered in IMR90 cells. Interestingly, protein phosphorylation of Rb (also known as Rb1) was inhibited in IMR90 cells (Fig. S4A). These results suggest that reduction of Rb protein phosphorylation is involved in TPPII-induced senescence. Nevertheless, our results suggest that neither the DNA damage-induced p53 nor the p21- or p16-mediated senescence pathway was activated in response to TPPII depletion in these normal cells. Consistent with these observations, no DNA damage response was induced in TPPII-depleting cells (Fig. S4B). Thus, these results suggest that TPPII depletion did not induce senescence through stimulating the conventional DNA damage response pathway.

The growth inhibition and phenotype changes accompanying TPPII depletion were not limited to normal lung fibroblast. Human normal skin fibroblast Detroit 551 also showed growth inhibition, activation of the SA-β-gal activity and reduction of BrdU incorporation upon TPPII depletion (Fig. 2F–I; Fig. S5A). Similar to what was observed in IMR90 cells, TPPII depletion did not induce the DNA damage response and its downstream p53, p21 or p16 pathway (Fig. S5B,C). It is well documented that telomere shortening is the main cause of replicative senescence (Allsopp et al., 1995; Bodnar et al., 1998). To assess whether TPPII depletion induced such a mechanism, we performed TPPII depletion study on telomerase-positive human normal fibroblast (BJ-hTERT) cells (Fig. 2J,K). The results showed that suppression of TPPII was able to induce senescence in BJ-hTERT cells, suggesting that TPPII does not induce senescence by affecting telomere length or telomerase activity.

SerpinB2 binds to TPPII and inhibits its activity

SerpinB2, also known as plasminogen activator inhibitor type 2 (PAI-2), is a serine protease inhibitor. It can extracellularly inhibit urokinase plasminogen activator (uPA, encoded by *PLAU*) and tissue plasminogen activator (tPA, encoded by *PLAT*) (Kruithof et al., 1986; Thorsen et al., 1988). In addition, serpinB2 participates in many cellular processes, including inflammation, fibrinolysis, extracellular matrix degradation, cell migration and invasion, wound healing and cleavage of specific cell surface proteins (Schroder et al., 2010). Recently, we demonstrated that serpinB2 has a direct role in senescence as we found that serpinB2 is upregulated in senescent cells and elevated levels of serpinB2 can induce senescence (Hsieh et al., 2017). These results were consistent with a previous reports on the involvement of serpinB2 in senescent human skin fibroblasts (Chen et al., 2004; Kumar et al., 1992; West et al., 1996; Zhang et al., 2003). Given that serpinB2 is a serine protease inhibitor, it is reasonable to speculate that serpinB2 might promote senescence by inhibiting its unidentified intracellular target serine proteases.

To test whether serpinB2 has a role in inhibiting TPPII activity during senescence, the interaction between TPPII and serpinB2 was first examined. Total cell extracts prepared from senescent IMR90 cells were immunoprecipitated with antibodies against TPPII and serpinB2, respectively. After PAGE and immunoblotting assays, the results from both co-immunoprecipitation experiments clearly confirmed that serpinB2 interacts with TPPII (Fig. 3A). To evaluate the functional consequence of the serpinB2–TPPII interaction, we first generated and purified recombinant serpinB2 from *Escherichia coli* (Fig. 3B). Applying the probe-based activity assay described above, we found that addition of recombinant serpinB2 to the cell extracts diminished the labeling of TPPII by probe **1** (Fig. 3C), indicating that TPPII activity is inhibited by serpinB2.

To determine whether an elevated level of serpinB2 inhibits TPPII in cells, serpinB2 was introduced into IMR90 cells and the TPPII activity was assessed via the activity assay described above. As shown in Fig. 3D, introducing the serpinB2-encoding gene into IMR90 cells resulted in decreased TPPII activities. It is also anticipated that lowering the serpinB2 level would lead to elevation of TPPII activity. To test this hypothesis, we depleted serpinB2 in IMR90 cells and determined the TPPII activity. We found TPPII activity was indeed increased in cells with lowed serpinB2 levels (Fig. 3E). Taken together, these results strongly support that TPPII is an intracellular target of serpinB2, and upregulation of serpinB2 suppresses TPPII activity in senescent cells.

TPPII inhibition activates TPPI activity

Interestingly, comparative proteomic analysis on senescent cells also revealed that the activity of TPPI, a lysosomal enzyme, was also increased (Table S1). This observation was in line with previous reports showing that the lysosomal enzyme activity is overactivated when cells are subjected to deletion or mutations of TPPII (Huai et al., 2008; Lu et al., 2014). We then proceeded to verify whether

Journal of Cell Science (2022) 135, jcs259513. doi:10.1242/jcs.259513

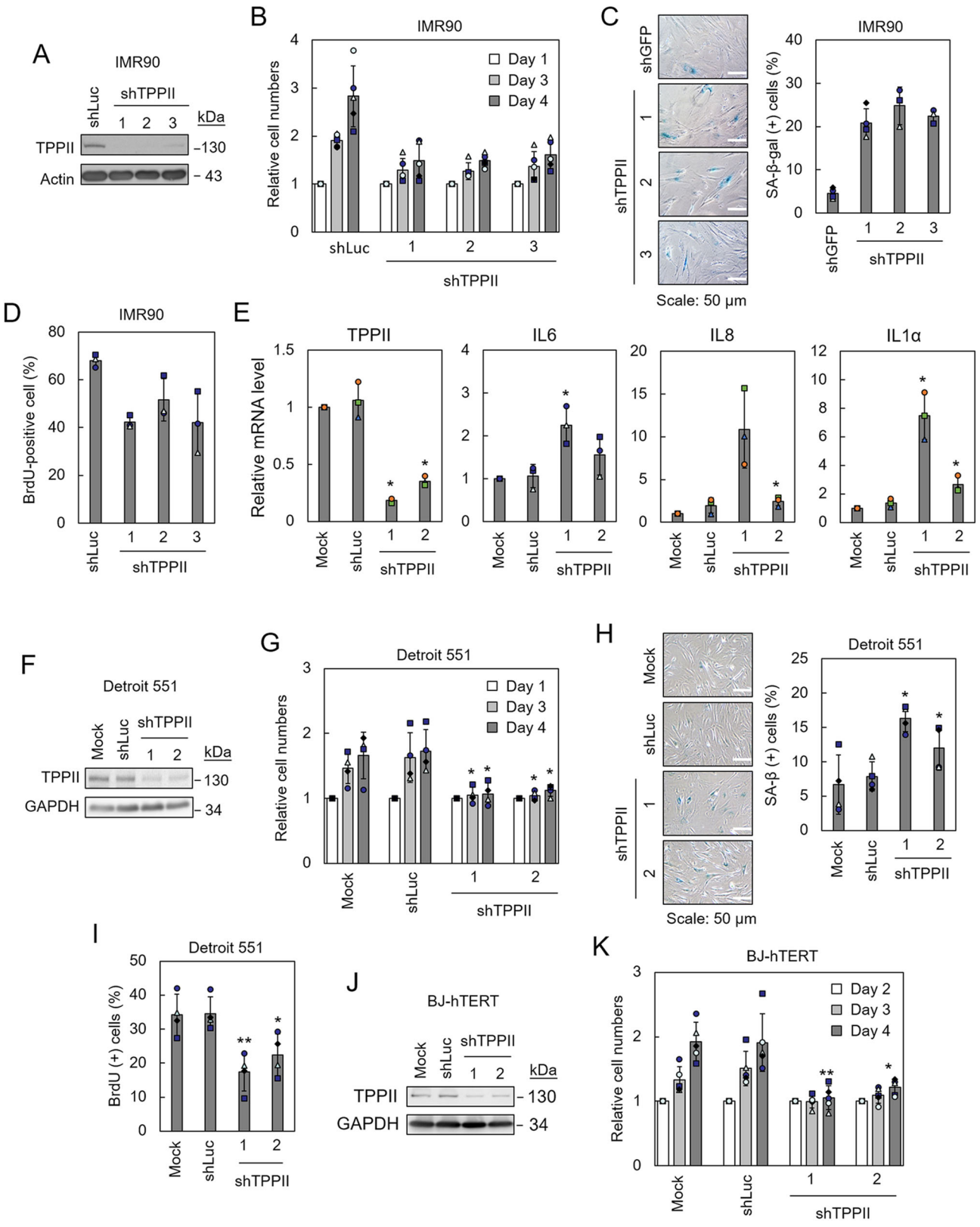

Fig. 2. See next page for legend.

TPPI is a downstream partner in the TPPII-mediated signaling axis. To test this hypothesis, we first evaluated the expression and activity of TPPI during senescence. As shown in Fig. 4A, the TPPI mRNA was slightly increased during senescence. By using the probe **1**-based activity assay protocol, we found that although the TPPI protein level was moderately increased, the activity of TPPI was significantly increased in senescent cells (Fig. 4B). Next, the effect of reducing levels of TPPII on TPPI was assessed. As shown in

Journal of Cell Science (2022) 135, jcs259513. doi:10.1242/jcs.259513

Fig. 2. Decreasing TPPII level induces senescence in IMR90 cells. (A) IMR90 cells were infected with shRNAs against TPPII (shTPPII) or Luc (shLuc). At 2 days after infection, puromycin (2 µg/ml) was added, followed by a further 2 days of incubation. Cell extracts were prepared from these cells and then separated using SDS-PAGE (8% gels). Immunoblotting analyses were conducted using antibodies against TPPII or actin. (B) Relative cell numbers were determined at the indicated times for the indicated knockdown cells. Results were obtained from the average of three independent experiments. (C) shTPPII- or shGFP-transduced cells were analyzed by SA-β-gal activity staining. Photographs of the X-gal-stained cells are shown (left). Quantification of the percentage of SA-β-gal positive-stained cells (right). Results were obtained from the average of three independent experiments. (D) The cells were cultured in medium containing BrdU, fixed and stained with anti-BrdU antibody. The cells were also stained with DAPI and visualized under a fluorescence microscope. The percentage of BrdU-positive cells is presented. Results were obtained from the average of three independent experiments. (E) Increased SASP upon SerpinB2 expression. IMR90 cells were transduced with adenovirus carrying SerpinB2 or LacZ. The cells were lysed and the mRNA levels were analyzed by qRT-PCR. The level of mRNA in LacZ-treated cells was set as 1. **P*<0.05. (F) Normal skin fibroblast Detroit 551 cells were infected with shRNAs against TPPII or Luc. Total cell extracts were prepared 3 days after infection and analyzed by immunoblotting assays using antibodies against TPPII or GAPDH. (G) The relative cell numbers of infected Detroit 551 cells were determined using Trypan Blue assays. (H) The senescence phenotype of infected Detroit 551 cells was analyzed by SA-β-gal assays 3 days after infection. The percentages of SA-β-gal-positive cells were quantified. (I) The percentage of infected Detroit 551 cells the were BrdU positive were quantified. (J) Telomerase immortalized BJ-hTERT cells were infected with shRNAs against TPPII or Luc. The cell lysates were separated and analyzed by SDS-PAGE (10%) followed by immunoblotting analysis using antibodies against TPPII or GAPDH. (K) The relative cell numbers for cells as in J were counted at the times indicated. Values show the average of three experiments. Quantification of results present in E, G, H, I and K were conducted from three to four independent experiments. Blot images in A, F and J are representative of three repeats. **P*<0.05; ***P*<0.01 (paired two-tailed Student's *t*-test).

Fig. 4C, the TPPI mRNA levels were moderately elevated in cells in TPPII knockdown conditions. Since TPPI is synthesized as a precursor protein and then auto-activated to form a mature enzyme at low pH (Lin et al., 2001), the TPPI protein level and the ratio between mature and precursor forms were measured. As shown in Fig. 4D,E, the TPPI protein levels were increased in cells with reduced TPPII levels. No apparent differences in the ratio of mature-to-precursor TPPI were found, indicating that TPPII does not affect TPPI maturation (Fig. 4F). The TPPI activity was also assessed using probe **1**-based activity assays. We found the TPPI activity was significantly increased in TPPII-depleted cells (Fig. 4G,H). Taken together, these results suggest that activation of TPPI activity is a consequence of TPPII reduction in senescent cells.

To study the role of TPPI in normal cells, we used an adenoviral delivering system to elevate the TPPI expression in normal fibroblasts. The TPPI levels in the TPPI-overexpressing cells were increased ∼3-fold (Fig. 4I). The cellular effects of increased TPPI expression were then evaluated in these normal fibroblasts. The proliferation potential was first examined. As shown in Fig. 4J, TPPI overexpression did not affect the proliferation of normal cells. At 4 days after infection, the morphology of TPPI-overexpressing cells appeared to be similar to that of proliferating cells (Fig. 4K, left panel). In line with this observation, the SA-β-gal activity was analyzed. The percentage of SA-β-gal positive cells was similar to that of mock-control and GFP-only-expressing cells (Fig. 4K, right panel). These results suggest that TPPI overexpression does not induce a senescence-like phenotype in normal fibroblasts. Thus, we conclude that TPPI is a downstream effector of TPPII and its activation is not sufficient to induce senescence.

The cellular lysosomal content has been reported to increase in human senescent fibroblasts (Comings and Okada, 1970; Lipetz and Cristofalo, 1972; Robbins et al., 1970). The same phenomenon has also been observed in senescent human umbilical vein endothelial cells (Kurz et al., 2000). Knowing the role of TPPII in proteostasis and that its suppression leads to activation of lysosomal TPPI, we thus evaluated the role of TPPII in lysosome homeostasis. The lysosomal contents of both young and senescent cells were determined by staining the cells with Lysotracker®. As shown in Fig. 5A, senescent cells showed higher lysosomal fluorescence intensity. The result is consistent with the published works showing that there is higher lysosomal contents in senescent cells. Similarly, the serpinB2-expressed senescent fibroblasts also showed a ∼2.5-fold lysosomal fluorescence intensity increase (Fig. 5B). It is important to note that the lysosomal fluorescent intensity was increased in TPPII-knockdown cells (Fig. 5C), supporting an inhibitory role of TPPII on the amount of lysosome contents. Therefore, these results show that TPPII also participates in regulating lysosome homeostasis.

DISCUSSION

Over the years, investigations have been performed on the alterations of mRNAs, microRNAs, proteins and phosphoproteins, as well as protein secretion, to discover novel factors involved in the senescent process (Acosta et al., 2008; Campisi and d'Adda di Fagagna, 2007; Chen et al., 2004; de Graaf et al., 2014; Grillari and Grillari-Voglauer, 2010; James et al., 2015; Kuilman et al., 2008; Kuilman and Peeper, 2009; Succoio et al., 2015; Zhang et al., 2003). Some success has indeed been achieved utilizing these conventional technical platforms. Nevertheless, these methods cannot address the dynamic alteration of enzymatic activities. The ability to identify activity alterations is especially important because many enzyme families participating in signaling pathways, including protein kinases, phosphatases, and serine proteases, are regulated post-translationally. These regulation events could be conducted through various processes such as protein–protein interactions, covalent modifications, cellular compartmentalization and proteolysis. Application of activity-based probes in profiling the alteration of enzymatic activities provides a powerful tool to identify important enzymes involved in cellular processes. By applying such a chemical proteomic approach, this study has successfully identified and elucidated the role of TPPII in senescence. Since the alterations of activities in other enzyme families during senescence are mostly uncharacterized, further development and application of chemical probes that target other enzyme families would greatly facilitate our understanding in senescence.

It has long been noted that serpinB2 expression level is elevated in senescent cells (Chen et al., 2004; Kumar et al., 1992; West et al., 1996; Zhang et al., 2003). It is a direct target of p53, which can be activated through a DNA damage response pathway (Hsieh et al., 2017). We have previously demonstrated that serpinB2 participates in the stabilization of p21 to inhibit cell proliferation in senescent cells (Hsieh et al., 2017). In this study, we further uncovered a new mode of action for serpinB2 in senescence. We found that serpinB2 can bind to TPPII and inhibit its activity, subsequently leading to the elevation of lysosomal content as well as activation of TPPI and β-galactosidase activities (Fig. 5D). Thus, this study reveals a signaling axis mediated through serpinB2-TPPII regulates lysosomal activity and proteostasis in senescence. Given that the serpinB2 level has also been found to be elevated upon application of different stresses in various cell types (Schroder et al., 2010; Zhang et al., 2015, 2009), our results imply that the newly unveiled

Journal of Cell Science (2022) 135, jcs259513. doi:10.1242/jcs.259513

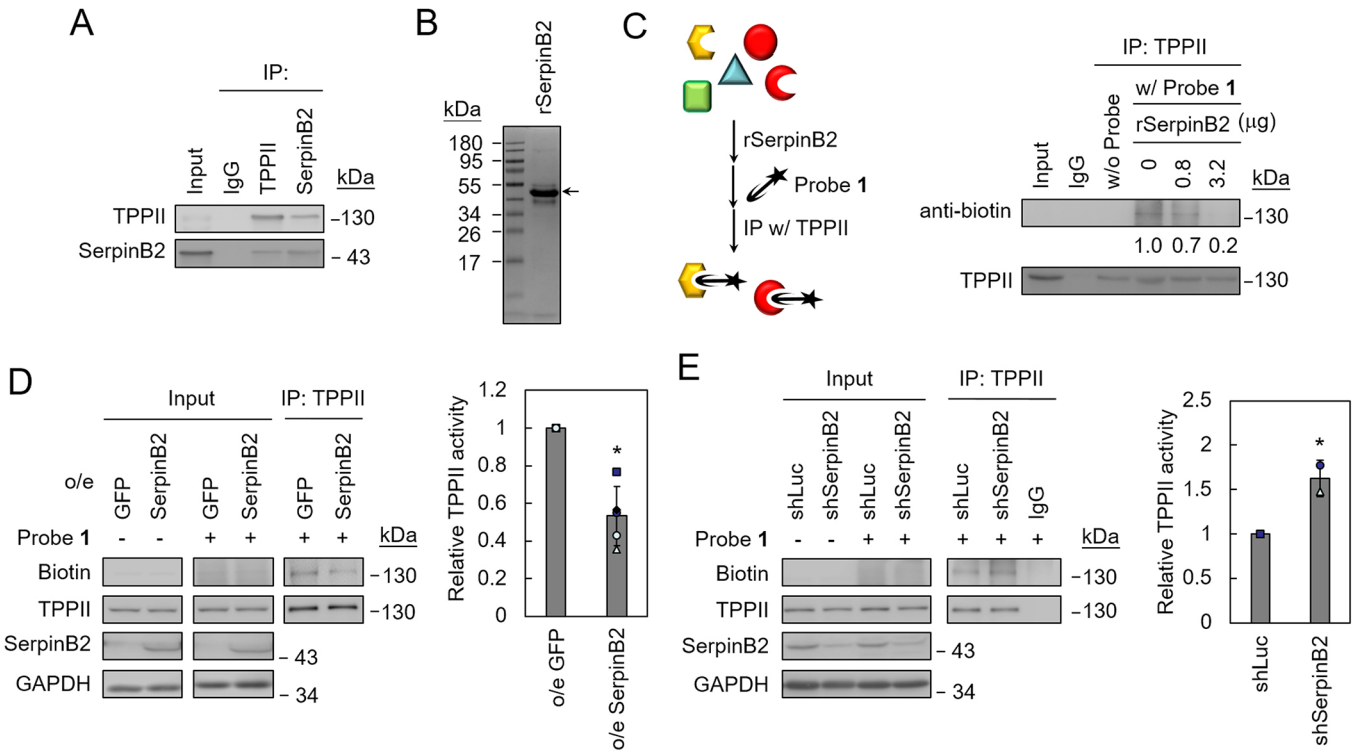

Fig. 3. SerpinB2 binds and inhibits TPPII. (A) Total cell extracts prepared from senescent IMR90 cells were immunoprecipitated with antibodies against TPPII or serpinB2. Immunoblotting assays were then conducted using antibodies against TPPII or serpinB2. (B) The 6-His tagged recombinant serpinB2 was expressed and isolated from *E. coli*. 1 µg of isolated serpinB2 proteins (rSerpinB2, recombinant SerpinB2) were separated by SDS-PAGE (10% gel) and stained with Coomassie Blue. (C) IMR90 cell extracts (80 µg) were treated with indicated amount of recombinant serpinB2 protein and then incubated with probe **1** (50 µM) at 25°C for 1 h. The probe-labeled proteins were immunoprecipitated with anti-TPPII antibody and then analyzed by immunoblotting assays using antibodies against biotin or TPPII. Blot image is representative of three repeats. (D) Cell lysates prepared from IMR90 cells expressing GFP or serpinB2, and were labeled with probe **1** (50 µM) at 25°C for 1 h. The probe **1**-labeled TPPII was immunoprecipitated by anti-TPPII antibody. The immunoprecipitated protein and activity of TPPII were assessed by immunoblotting with anti-TPPII and biotin antibodies, respectively. Quantification of the TPPII activities was assessed relative to the level of shLuc, which was set as 1. Results were obtained from the average of three independent experiments. (E) Cell extracts were prepared from IMR90 cells that had been transfected with shLuc or shSerpinB2. The TPPII activities were then analyzed as in D. **P*<0.05 (paired two-tailed Student's *t*-test). Input lanes in C–E represent 10% of protein used for IP. w/, with; w/o, without; o/e, overexpressing.

serpinB2-TPPII signaling axis may also have roles in response to different stresses. It is also interesting to note that TPPII-depleted cells did not induce DNA damage response, nor activate a p53-, p21- or p16-mediated pathway. The results are consistent with our finding that TPPII functions downstream of serpinB2 to regulate senescence.

One of the most characteristic changes observed in senescent fibroblasts is the increase in lysosomal number and size (Comings and Okada, 1970; Lipetz and Cristofalo, 1972; Robbins et al., 1970). As a result, lysosomal β-galactosidase levels are elevated in senescent cells (SA-β-gal), and this has become the most extensively utilized biomarker of senescent or aged cells (Dimri et al., 1995; Kurz et al., 2000; Lee et al., 2006). In this study, we found that inactivation of TPPII by serpinB2 could lead to increased lysosome contents as well as elevation of lysosomal enzymes including TPPI and SA-β-gal. These results might provide explanation for a long-standing puzzle of how SA-β-gal activity is activated in senescent cells. Interestingly, a previous report has also revealed a role for TPPII in lysosomal activation (Lu et al., 2014). It showed that TPPII mutations caused defects in amino acid homeostasis, leading to lysosomal overactivity and reduced glycolysis in human T cells. Data in this study further established that TPPII has a role in cellular senescence and that its reduction is sufficient to induce senescence in normal human fibroblasts, confirming the pivotal role of TPPII in lysosomal activation and proteostasis. The finding is also consistent with the general notion that failed maintenance of protein homeostasis or proteostasis can cause stress in cells to induce senescence or aging (Kaushik and Cuervo, 2015).

The mechanism of how TPPI is activated is less clear. Given that cells with TPPII mutations are characterized by defects in proteostasis (Lu et al., 2014), elevation of TPPI protein level and activity might be simply due to an adaptive effect to compensate for defect in protein homeostasis. This notion is supported by studies showing that TPPI is a downstream target of transcription factor EB (TFEB) and inactivation of TPPII induces translocation of TFEB into nucleus (Lu et al., 2014; Sardiello et al., 2009). Thus, it is likely that the elevated TPPI expression is due to activation of TFEB upon TPPII inhibition in senescent cells. Alternatively, global genome analysis for p53-binding sites has found that TPPI is a direct downstream target gene of p53, whose level can be activated by DNA damaging agents (Kenzelmann Broz et al., 2013). Thus, activation of p53 might also contribute to TPPI activation in senescent cells.

In summary, we have applied a chemical proteomic approach to identify serine proteases whose activities were altered during senescence. We have also showed that TPPII is an intracellular target of serpinB2 and that its activity is inhibited when serpinB2 level is elevated in senescent cells. Importantly, we found that the serpinB2-TPPII signaling axis is involved in downstream

Journal of Cell Science (2022) 135, jcs259513. doi:10.1242/jcs.259513

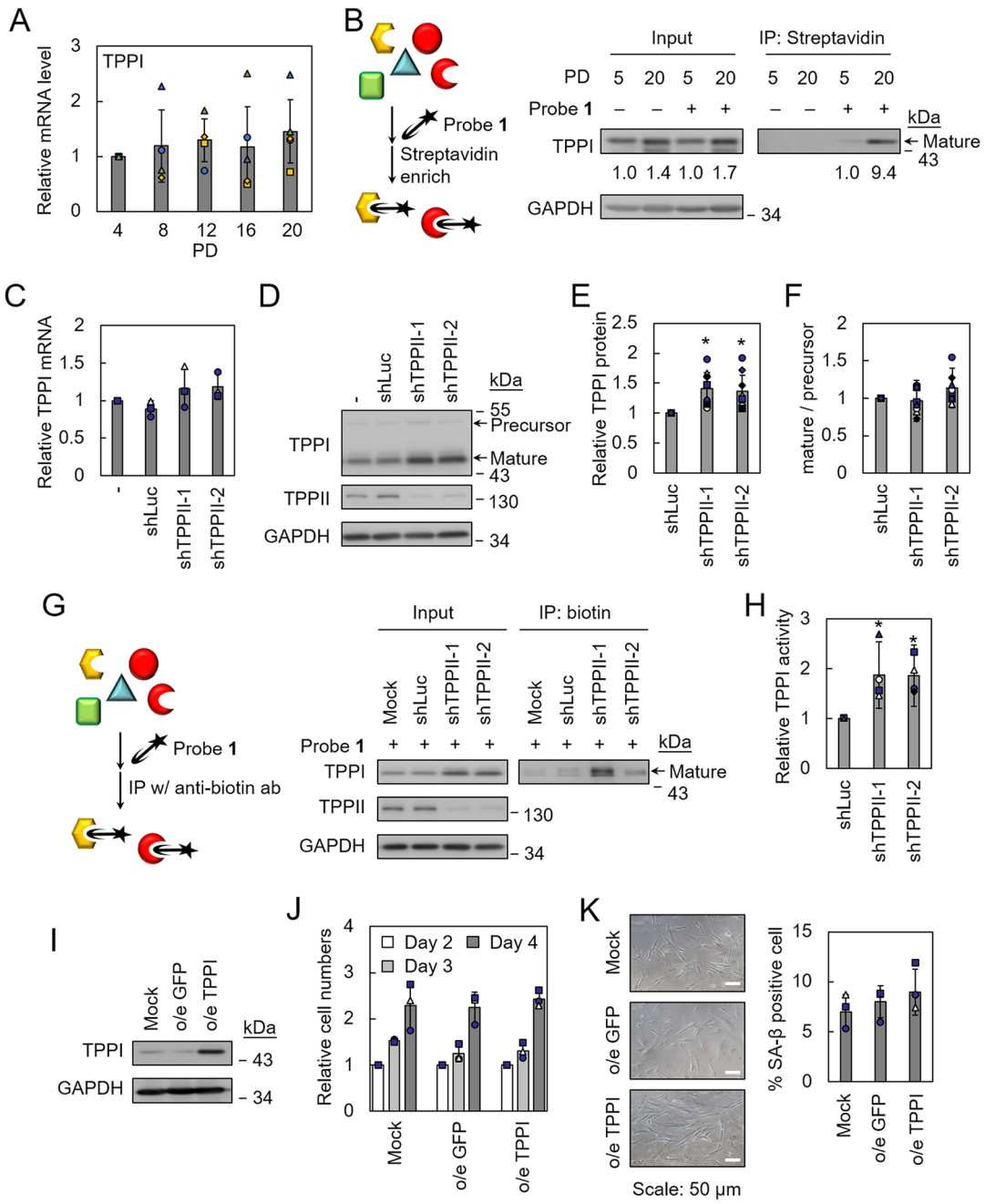

Fig. 4. Activation of TPPI activity by TPPII depletion. (A) The mRNA levels of TPPI in young and senescent IMR90 cells. RNA from IMR90 cells with PD at 4, 8, 12, 16, and 20 were prepared and analyzed by qRT-PCR. GAPDH was used as an internal control and all samples were normalized to GAPDH. The values were obtained from the average of four independent experiments. Error bars represent s.d. (B) Cell lysates prepared from IMR90 cells at PD5 (young) and PD20 (senescent) were labeled with probe **1** (50 μM) at 25°C for 1 h. The probe **1**-labeled TPPI was pulled down by streptavidin beads, eluted with 2% SDS, and then separated by SDS-PAGE (10% gels). The activity levels of TPPI proteins (numbers below blots) were determined by immunoblotting analysis using anti-TPPI antibody, and represent normalized optical density of three independent experiments. (C) The mRNA levels of TPPI in TPPII-depleted (shTPPII) IMR90 cells. Total mRNAs were prepared 4 days after infecting IMR90 cells with shRNAs against TPPII or Luc and analyzed by qRT-PCR. GAPDH was used as an internal control and all samples were normalized to GAPDH. The values were obtained from the average of three independent experiments. Error bars represent s.d. (D) As in C, immunoblotting assays were used to analyze the protein levels of TPPII, TPPI or GAPDH for the indicated cells. (E) Quantification of the mature TPPI protein levels. (F) The relative levels of mature and precursor forms of TPPI were quantified for the indicated cells. (G) Total cell extracts were prepared from TPPII-depleted IMR90 cells. These cell lysates were labeled with probe **1** (50 μM) at 25°C for 1 h. The probe **1**-labeled TPPI was pulled down by anti-biotin antibody, eluted with 2% SDS, and then separated by SDS-PAGE (10% gels). The activity levels of TPPI proteins were determined by immunoblotting analysis using anti-TPPI antibody. (H) Quantification of TPPI activity in TPPII-depleted cells. The values were obtained from the average of four independent experiments. Error bars represent s.d. **P*<0.05 (paired two-tailed Student's *t*-test). (I) IMR90 cells were infected with adenovirus carrying GFP or TPPI. (o/e; overexpressing). Cell extracts were prepared from these cells and then separated using 10% SDS-PAGE. Immunoblotting analyses were conducted using antibodies against TPPI or GAPDH. (J) The relative cell numbers for cells as in I were determined at the indicated times. Results were obtained from the average of three independent experiments. (K) TPPI- or GFP-overexpressing cells were analyzed by SA-β-gal activity staining. Photographs of the X-gal-stained cells are shown (left). Quantification of the percentage of SA-β-gal positive-stained cells was conducted (right). Results were obtained from the average of three independent experiments. Blot images in B, D, G and I are representative of three repeats. Input lanes in B and G represent 10% of protein used for IP.

Journal of Cell Science

Journal of Cell Science (2022) 135, jcs259513. doi:10.1242/jcs.259513

physiological changes in senescence. Given that serpinB2 is a direct downstream target of p53, which is frequently activated by many stressors, this study further implies that the serpinB2-TPPII signaling axis could serve as a pivotal mechanism to relay the stress signals.

MATERIALS AND METHODS

Labeling reactions of probe 1

The synthesis of probe **1** and the detailed experimental procedures are as described in Liao, 2009. In labeling purified proteins, 1 µg protein was incubated with 1 or 3 µM of probe **1** in reaction buffer containing 50 mM Tris-HCl pH 8.0, 1 mM EDTA and 50 mM NaCl at 25°C for 10 min. The reaction products were separated by SDS-PAGE (10% gels) and transferred onto a nitrocellulose membrane. The membrane was blocked with 10% nonfat dry milk, washed with 0.05% Tween-20, 20 mM Tris-HCl pH 7.6, 137 mM NaCl (TTBS), and then treated with a streptavidin-horseradish peroxidase conjugate (Amersham-Pharmacia, 1:2000 dilution) in TTBS with 1% nonfat dry milk for 1 h at 25°C. Visualization of bound streptavidin-horseradish peroxidase conjugate was achieved by treating the membrane with ECL chemiluminescence reagents (Amersham-Pharmacia) and exposed to film for 0.5–30 min before development. For labeling cell extracts, IMR90 cells were washed with cold PBS and then resuspended in buffer containing 50 mM Tris-HCl pH7.5, 100 mM NaCl, 0.1% SDS, 1% Triton X-100 and 5 mM EDTA and then sonicated to disrupt the cells. Total cell extracts were then collected by centrifugation under 16,000 ***g*** at 4°C for 10 min. The concentration of protein in cell extracts was determined using a Bio-Rad protein assay kit with bovine serine albumin as a standard. Cell extracts were then incubated with 50 µM of probe **1** at 25°C for 1 h.

Cell lines and cell culture

The normal human lung fibroblast line IMR90, normal human skin fibroblast line Detroit 551, and telomerase-immortalized human normal skin fibroblast line BJ-hTERT were purchased from the Food Industry Research and Development Institute (Taiwan). The human embryonic kidney cell line HEK293T was a gift from the lab of Dr Helene M. Liu (Biochemistry and Molecular Biology, National Taiwan University College of Medicine). The AD293 cell line (derived from the standard HEK293 cell line) was purchased from Agilent Technolobies. IMR90 and Detroit 551 cells were maintained in minimum essential medium (MEM, Gibco Thermo Fisher Scientific Inc.) containing 10% fetal bovine serum (FBS). BJ-hTERT, HEK293T and AD293 cells were maintained in Dulbecco's modified Eagle medium (DMEM, Gibco Thermo Fisher Scientific Inc.) containing 10% FBS. The purchased IMR90 cells and Detroit 551 cells could be cultured for additional ∼20 passages and ∼15 passages before showing sign of senescence, respectively. In this study, both proliferation rate and senescence-associated β-galactosidase activity (SA-β-gal) were used to evaluate the senescence status of IMR90 and Detroit 551. If the percentage of SA-β-gal-positive cells was less than 10%, cells were considered 'young'. Cells were classed as 'senescent' when over 30% were positive for SA-β-gal.

Gene knockdown by shRNAs

The shRNAs used in this study were purchased from RNA Technology Platform and Gene Manipulation core (RNAi core) at Academia Sinica, Taiwan. In typical knockdown experiments, cells were transduced with shRNAs against target or control genes. The infected cells were then recovered with fresh growth medium for 1 day, and selected with 0.8 µg/ml puromycin for another 2 days before analysis. The sequences

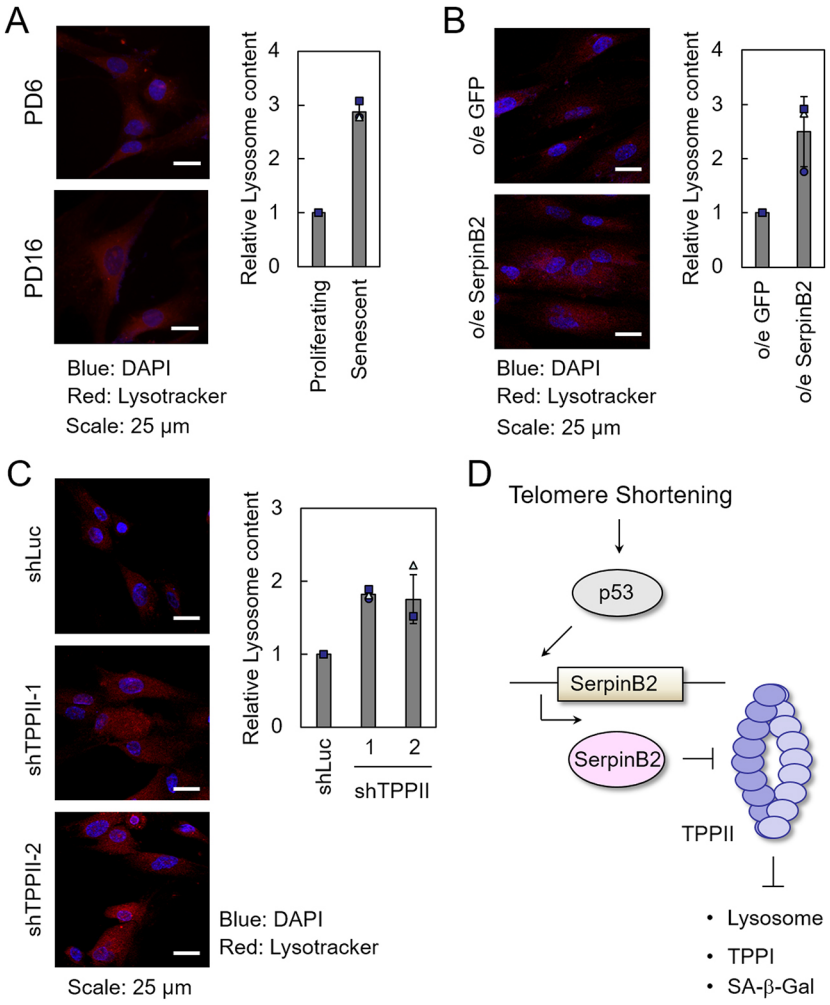

Fig. 5. Depleting of TPPII induces an increase in lysosome content. (A) IMR90 cells with PD at 6 and 16 were analyzed for lysosome content using Lysotracker (red). These cells were also stained with DAPI to locate the position of nuclei (blue). Images of the cells were taken by a confocal microscope (left). The Lysotracker fluorescence signals were quantified and the relative lysosome content were determined relative to cells at PD6, set at 1 (right). Results were obtained from the average of three independent experiments. (B) Overexpression (o/e) of serpinB2 induced an increase in lysosome content. IMR90 cells were transduced with adenovirus carrying the SerpinB2 or GFP. The SerpinB2- or GFP-transduced cells were analyzed for lysosome content. The Lysotracker fluorescence signals were quantified and the relative lysosome content was determined relative to cells expressing GFP, which was set as 1 (right). Results were obtained from the average of three independent experiments. (C) IMR90 cells carrying shRNAs against TPPII or Luc were analyzed for lysosome content. The images (left) and relative lysosome content (right) are presented. The relative lysosome contents were determined relative to cells carrying shLuc, which was set as 1. Results were obtained from the average of three independent experiments. (D) Model for the involvement of serpinB2-TPPII in senescence.

Journal of Cell Science (2022) 135, jcs259513. doi:10.1242/jcs.259513

for the target genes are: shTPPII-1, 5′-GCTGGATTCTAGTGACATTTA-3′; shTPPII-2, 5′-CGCCTTAAAGACCTTCCATTT-3′; shTPPII-3, 5′-CCTGATCCTTTCAGGTCTGAA-3′; shSerpinB2, 5′-GCAGATCCA-GAAGGGTAGTTA-3′; shLuc, 5′-CTTCGAAATGTCCGTTCGGTT-3′; and shGFP, 5′-CCCGACCACATGAAGCAGCAC-3′.

Gene overexpression via the adenoviral expression system

The AdEasy Adenoviral Vector System (Agilent Technologies) was used to prepare adenoviral expressed genes. Briefly, the cDNA of GFP, serpimB2 or TPPI was amplified from cDNA prepared from IMR90 cells, and cloned into pShuttle-CMV plasmid. The resulting constructs were then transformed into *E. coli* BJ5183-AD-1 cells to prepare the recombinant viral DNA plasmids. These recombined viral DNA plasmids were then linearized with PacI and transfected into AD293 cells to assemble recombinant viral particles. In the overexpression experiments, cells were infected with recombinant adenovirus for 2 days and then analyzed.

Activity probe-based protease activity analysis

Total cell lysates prepared from PD5 (young) and PD20 (senescent) IMR90 cells were adjusted to 1 mg/ml protein concentration with the Tris buffer and then incubated with probe **1** for labeling. In a typical reaction, 500 µg of cell extract was incubated with 50 µM probe **1** at 25°C for 1 h. Streptavidin beads were added to pull down probe **1**-labeled proteins. The pulled down proteins were separated by 10% SDS-PAGE. The amount and the activity of the corresponding protease was determined by immunoblotting analysis using anti-target and anti-biotin antibody, respectively. For TPPII, antibody (3 µg; 1:2000, 14120-1-AP, Proteintech) against TPPII was added into the reaction mixtures at 4°C for 2 h to immunoprecipitate TPPII. The precipitated proteins were then separated by 10% SDS-PAGE. Detection of TPPII precipitation efficiency and the extent of probe **1** labeling were conducted using immunoblotting analysis as described earlier.

For the inhibition analysis of TPPII activity by serpinB2, the 6-His tagged recombinant serpinB2 was isolated from *E. coli* and used in the analysis as described previously (Hsieh et al., 2017). Cell extracts prepared from PD5 IMR90 cells (80 µg) were mixed with recombinant serpinB2 protein (0.8 or 3.2 µg) and then incubated with probe **1** (50 µM) at 25°C for 1 h. The probe-labeled proteins were immunoprecipitated with anti-TPPII antibodies and then separated by 10% SDS-PAGE. Immunoblotting analyses were conducted using antibodies against biotin or TPPII.

Growth curves

The proliferative capacity of cells was monitored by seeding 7.5×10^5 cells into a 100-mm dish containing 10% FBS. Cell numbers were determined by digesting the cells with trypsin, stained with 0.2% Trypan Blue, and counted using a hemocytometer.

BrdU incorporation analysis

Cells were cultured in medium containing 10 µM BrdU for 24 h. After labeling, the cells were fixed and stained with anti-BrdU antibody. BrdU-positive cells were detected by counterstaining with DAPI and visualized under a fluorescence microscope.

SA-β-galactosidase staining

Cells were washed with PBS (137 mM NaCl, 2.7 mM KCl, 10 mM Na_2HPO_4, 1.8 mM KH_2PO_4, pH 7.4) and fixed for 10 min in 2% formaldehyde and 0.2% glutaraldehyde. The fixed cells were then incubated with staining solution (40 mM citrate, 5 mM potassium ferrocyanide, 5 mM potassium ferricyanide, 150 mM NaCl, 2 mM $MgCl_2$ and sodium phosphate, pH 6.0) containing 1 mg/ml 5-bromo-4-chloro-3-indolyl-β-D-galactoside (X-Gal) at 37°C for 16–24 h. At least 250 cells were counted in randomly chosen fields for each sample.

Lysosome content determination

About 2×10^4 IMR90 cells were incubated with 100 nM LysoTracker® (Life Technologies) at 37°C for 5 h. The cells were then fixed with 2% formaldehyde and counterstained with DAPI. For the TPPII-knockdown cells, 8×10^4 IMR90 cells were infected with shRNAs against luciferase or TPPII. The infected cells were selected with 0.8 µg/ml puromycin and then stained with LysoTracker®. For serpinB2 overexpression experiments, IMR90 cells were infected with adenovirus containing GFP or SerpinB2 and then stained with LysoTracker®. The cells were then observed under a confocal microscope (Leica TCS SP5). The excitation wavelengths for Lysotracker Red and DAPI were 561 nm and 405 nm, respectively. The images were collected and processed by LAS X Life Science Microscope software. The Lysotracker Red intensity was analyzed and quantified by software ImageJ.

Labeling and identification of probe 1-labeled proteins by mass spectrometry

Cell lysates from young and senescent IMR90 cells were labeled with 50 µM of probe **1** for 1 h at 25°C. Unbound free probes were removed by PD-10 column and the probe **1**-labeled proteins were then pulled down by streptavidin-coated magnetic beads (GE Healthcare). The labeled proteins were then eluted with 2% SDS and heated at 95°C for 5 min followed by gel-assisted digestion (Han et al., 2008). In brief, the proteins were reduced by 5 mM tris(2-carboxyethyl)phosphine (TCEP) at 37°C for 30 min and alkylated by 10 mM iodoacetamide (IAM) at 37°C for 1 h in the dark. To incorporate proteins into a gel directly in the Eppendorf vial, the volume ratio (14:5:0.7:0.3) of sample:acrylamide/bisacrylamide solution (40%, v/v, 29:1): 10% (w/v) APS: 100% TEMED was then added, and the gels were allowed to stand at room temperature for at least 30 min. The gels were cut into small pieces and washed several times with 1 ml of 20 mM TEABC containing 50% (v/v) CH_3CN. The gel samples were further dehydrated with 100% CH_3CN and then completely dried with a SpeedVac. The gel was resuspended in 25 mM TEABC and then incubated with trypsin (protein/trypsin=10/1, w/w) at 37°C overnight. Peptides were further extracted from the gel using 5% (v/v) formic acid (FA) in 50% CH_3CN twice and 100% CH_3CN. The peptides were combined, concentrated in a SpeedVac, and desalted by C18 Ziptip (Millipore).

LC-MS/MS analysis and protein identification

Nano-liquid chromatography none-electrospray ionization tandem mass spectrometry (NanoLC-nanoESI-MS/MS) analysis was performed on a nanoAcquity system (Waters, Milford, MA) connected to the Orbitrap Velos hybrid mass spectrometer (Thermo Fisher Scientific, Bremen, Germany) equipped with a PicoView nanospray interface (New Objective, Woburn, MA). Peptide mixtures were loaded onto a 75 µm internal diameter (ID), 25 cm length C18 BEH column (Waters, Milford, MA) packed with 1.7 µm particles with a pore with of 130 Å, and were separated using a segmented gradient in 120 min from 5% to 40% solvent B (CH_3CN with 0.1% FA) at a flow rate of 300 nl/min and a column temperature of 35°C. Solvent A was 0.1% FA in water. The mass spectrometer was operated in the data-dependent mode. Briefly, survey full scan MS spectra were acquired in the orbitrap (m/z 350–1600) with the resolution set to 60 K at m/z 400 and automatic gain control (AGC) target at 10^6. The 20 most intense peptide ions with charge states ≥2 were sequentially isolated to a target value of 5000 and fragmented in the high-pressure linear ion trap by low-energy collision-induced dissociation (CID) with normalized collision energy of 35%. The resulting fragments were scanned out in the low-pressure ion trap at the normal scan rate and recorded with the secondary electron multipliers. The ion selection threshold was 2000 counts for MS/MS, and the maximum allowed ion accumulation times were 200 ms for full scans and 50 ms for CID-MS/MS measurements in the LTQ. An activation q=0.25 and activation time of 10 ms were used. The raw data were processed by using Proteome Discoverer 2.1 (PD2.1; Thermo Fisher Scientific), and peptide identification was performed by Mascot search engine (version 2.3.2) and SEQUEST search engine against the Swiss-Prot database (v2015_12, total 20,193 sequences from human) with a percolator [strict false discovery rate (FDR) of 0.01 and a relaxed FDR of 0.05]. The protease was specified as trypsin with two maximum missing cleavage sites. Mass tolerance for precursor ion mass was 10 ppm with the fragment ion tolerance as 0.1 Da. Oxidation at methionine, carbamidomethyl at cysteine, and deamidation at

asparagine or glutamine, were selected as variable modifications. Peptides were considered to be identified if their individual ion score was higher than the identity score (P<0.05). To evaluate the FDR (<1%) in protein identification, a decoy database search against a randomized decoy database created by PD2.1 using identical search parameters and validation criteria was also performed. Peptide-spectrum matches (PSMs) with at least high confidence and a strict maximum parsimony principle (target FDR <0.01) were applied for the protein level. For label-free quantitation, the peak area (i.e. area under the curve) of each precursor ion was calculated from extracted ion chromatogram during data processing by using the Precursor Ions Area Detector node with mass precision 2 ppm. The abundance of identified protein was calculated from top three of all unique and razor peptides in Peptide and Protein Quantifier node. The relative quantitation was further compared with the protein abundance from young and senescent samples.

Immunoblotting analysis

Cells were lysed in RIPA buffer (Tris-HCl pH 7.4 50 mM, NP-40 1%, sodium deoxycholate 0.5%, SDS 0.1%, NaCl 150 mM) containing 1 mM PMSF and protease inhibitor cocktail (539134, Calbiochem) and the proteins were separated by SDS-PAGE (8%, 10%, 12% or 15% gels). The proteins were transferred onto nitrocellulose membranes and probed with anti-biotin (1:5000, ab53494, Abcam), anti-TPPI (1:2000, sc-365838, Santa Cruz Biotechnology), or anti-TPPII (1:2000, 14120-1-AP, Proteintech). Bound antibodies were visualized by chemiluminescence using an ECL kit (Amersham Biosciences). The luminescence intensities were determined by ImageJ. Quantification of the relative levels was determined from at least three independent experiments.

qRT-PCR

The total amount of RNA was extracted by GENEzol™ Reagent (Geneaid). First-strand cDNA was synthesized from 0.5 µg of total RNA with RevertAid RT Reverse Transcription Kit (Thermo Scientific). Real-time PCR was then performed using SYBR Green Master Mix (Roche) and StepOne Real-Time PCR System (Applied Biosystems). The primer pairs are: TPPI, 5′-GGCAGGACTCTTTGATGTAACC-3′ and 5′-TGATAGGA-AAGGGTCAGGGGT-3′; TPPII, 5′-GTCTGGAGAGCCTGCATTGA-3′ and 5′-CTCAGCTGTGCCAAAAGAGC-3′; IL6, 5′-CAGGAGCCCAGC-TATGAACT-3′ and 5′-GAAGGCAGCAGGCAACAC-3′; IL8, 5′-GAG-TGGACCACACTGCGCCA-3′ and 5′-TCCACAACCCTCTGCACCC-AGT-3′; IL1α, 5′-GCTGAAGGAGATGCCTGAGAT-3 and 5′-GCAC-ACCCAGTAGTCTTGCTT-3; and GAPDH, 5′-GAAGGTGAAGGT-CGGAGTCAA-3′ and 5′-CGTTCTCAGCCTTGACGGT-3′). GAPDH was used as an internal control and all samples were normalized to GAPDH.

Statistical analysis

A paired two-tailed Student's t-test was applied to assess whether the means of two groups are statistically different from each other. We consider P<0.05 as significant.

Acknowledgements

Mass spectrometry analyses were performed by the Academia Sinica Common Mass Spectrometry Facilities located at the Institute of Biological Chemistry, Academia Sinica, Taiwan. The shRNAs were obtained from the RNA Technology Platform and Gene Manipulation core (RNAi core) at Academia Sinica, Taiwan. Image acquisition and analysis was provided by the imaging core at the First Core Labs, National Taiwan University College of Medicine. The human embryonic kidney cell line HEK293T was a kind gift from Dr Helene Minyi Liu at the Institute of Biochemistry and Molecular Biology, National Taiwan University College of Medicine.

Competing interests

The authors declare no competing or financial interests.

Author contributions

Conceptualization: L.-C.L., J.-J.L.; Methodology: C.-L.L., R.-C.H., M.-S.L., Y.-P.C., H.-H.H., C.-H.T., T.-C.C., C.-Y.C.; Validation: C.-L.L., Y.-P.C.; Formal analysis: C.-L.L., R.-C.H., M.-S.L., Yi-J.C.; Investigation: C.-L.L., R.-C.H., M.-S.L., Yi-J.C., Y.-P.C., C.-H.T.; Resources: Yi-J.C., Yu-J.C.; Data curation: C.-L.L., M.-S.L.; Writing - original draft: L.-C.L., J.-J.L.; Writing - review & editing: L.-C.L., J.-J.L.; Visualization: J.-J.L.; Supervision: L.-C.L., J.-J.L.; Project administration: L.-C.L., J.-J.L.; Funding acquisition: J.-J.L.

Funding

This research was supported by Ministry of Science and Technology grants (MOST 107-3017-F-002-002 and 109-2311-B-002-014-MY3 to J.-J.L., and MOST 102-2113-M-002-004-MY3 and 105-2113-M-002-006 to L.-C.L.). This work was also supported by the "Center of Precision Medicine" from The Featured Areas Research Center Program within the framework of the Higher Education Sprout Project by the Ministry of Education (MOE) in Taiwan.

Data availability

The mass spectrometry proteomics data have been deposited to the ProteomeXchange Consortium via the PRIDE (Perez-Riverol et al., 2022) partner repository with the dataset identifiers PXD033808.

Peer review history

The peer review history is available online at https://journals.biologists.com/jcs/article-lookup/doi/10.1242/jcs.259513.

References

Acosta, J. C., O'Loghlen, A., Banito, A., Guijarro, M. V., Augert, A., Raguz, S., Fumagalli, M., Da Costa, M., Brown, C., Popov, N. et al. (2008). Chemokine signaling via the CXCR2 receptor reinforces senescence. *Cell* **133**, 1006-1018. doi:10.1016/j.cell.2008.03.038

Allsopp, R. C., Chang, E., Kashefi-Aazam, M., Rogaev, E. I., Piatyszek, M. A., Shay, J. W. and Harley, C. B. (1995). Telomere shortening is associated with cell division *in vitro* and *in vivo*. *Exp. Cell Res.* **220**, 194-200. doi:10.1006/excr.1995.1306

Autefage, H., Albinet, V., Garcia, V., Berges, H., Nicolau, M.-L., Therville, N., Altié, M.-F., Caillaud, C., Levade, T. and Andrieu-Abadie, N. (2009). Lysosomal serine protease CLN2 regulates tumor necrosis factor-α-mediated apoptosis in a Bid-dependent manner. *J. Biol. Chem.* **284**, 11507-11516. doi:10.1074/jbc.M807151200

Balow, R.-M., Tomkinson, B., Ragnarsson, U. and Zetterqvist, O. (1986). Purification, substrate specificity, and classification of tripeptidyl peptidase II. *J. Biol. Chem.* **261**, 2409-2417. doi:10.1016/S0021-9258(17)35951-3

Bodnar, A. G., Ouellette, M., Frolkis, M., Holt, S. E., Chiu, C.-P., Morin, G. B., Harley, C. B., Shay, J. W., Lichtsteiner, S. and Wright, W. E. (1998). Extension of life-span by introduction of telomerase into normal human cells. *Science* **279**, 349-352. doi:10.1126/science.279.5349.349

Campisi, J. and d'Adda di Fagagna, F. (2007). Cellular senescence: when bad things happen to good cells. *Nat. Rev. Mol. Cell Biol.* **8**, 729-740. doi:10.1038/nrm2233

Cárcel-Trullols, J., Kovács, A. D. and Pearce, D. A. (2015). Cell biology of the NCL proteins: what they do and don't do. *Biochim. Biophys. Acta* **1852**, 2242-2255. doi:10.1016/j.bbadis.2015.04.027

Chen, H.-L., Lu, C.-Y., Hsu, Y.-H. and Lin, J.-J. (2004). Chromosome positional effects of gene expressions after cellular senescence. *Biochem. Biophys. Res. Commun.* **313**, 576-586. doi:10.1016/j.bbrc.2003.11.146

Chu, C.-Y., Kuo, C.-C., Chen, M.-H., Chen, K.-J., Lo, L.-C. and Lin, J.-J. (2012). Development of a plate-based assay platform to monitor cellular SHP2 phosphatase activity during erythroid differentiation. *J. Chin. Chem. Soc.* **59**, 297-304. doi:10.1002/jccs.201100725

Comings, D. E. and Okada, T. A. (1970). Electron microscopy of human fibroblasts in tissue culture during logarithmic and confluent stages of growth. *Exp. Cell Res.* **61**, 295-301. doi:10.1016/0014-4827(70)90451-9

de Graaf, E. L., Kaplon, J., Zhou, H., Heck, A. J. R., Daniel, S., Peeper, D. S. and Altelaar, A. F. M. (2014). Phosphoproteome dynamics in onset and maintenance of oncogene-induced senescence. *Mol. Cell. Proteomics* **13**, 2089-2100. doi:10.1074/mcp.M113.035436

Dimri, G. P., Lee, X., Basile, G., Acosta, M., Scott, G., Roskelley, C., Medrano, E. E., Linskens, M., Rubelj, I., Pereira-Smith, O. et al. (1995). A biomarker that identifies senescent human cells in culture and in aging skin *in vivo*. *Proc. Natl. Acad. Sci. USA* **92**, 9363-9367. doi:10.1073/pnas.92.20.9363

Gavioli, R., Frisan, T., Vertuani, S., Bornkamm, G. W. and Masucci, M. G. (2001). c-*myc* overexpression activates alternative pathways for intracellular proteolysis in lymphoma cells. *Nat. Cell Biol.* **3**, 283-288. doi:10.1038/35060076

Grillari, J. and Grillari-Voglauer, R. (2010). Novel modulators of senescence, aging, and longevity: Small non-coding RNAs enter the stage. *Exp. Gerontol.* **45**, 302-311. doi:10.1016/j.exger.2010.01.007

Han, C.-L., Chien, C.-W., Chen, W.-C., Chen, Y.-R., Wu, C.-P., Li, H. and Chen, Y.-J. (2008). A multiplexed quantitative strategy for membrane proteomics: opportunities for mining therapeutic targets for autosomal dominant polycystic kidney disease. *Mol. Cell. Proteomics* **7**, 1983-1997. doi:10.1074/mcp.M800068-MCP200

Hayflick, L. (1965). The limited *in vitro* lifetime of human diploid cell strains. *Exp. Cell Res.* **37**, 614-621. doi:10.1016/0014-4827(65)90211-9
Hayflick, L. and Moorhead, P. S. (1961). The serial cultivation of human diploid cell strains. *Exp. Cell Res.* **25**, 585-621. doi:10.1016/0014-4827(61)90192-6
Hsieh, H.-H., Chen, Y.-C., Jhan, J.-R. and Lin, J.-J. (2017). Serine protease inhibitor SerpinB2 binds and stabilizes p21 in senescent cells. *J. Cell. Science* **130**, 3272-3281. doi:10.1242/jcs.204974
Hsu, Y.-L., Yang, C.-C., Chou, T.-C., Tai, C.-H., Chen, L.-Y., Fu, S.-L., Lin, J.-J. and Lo, L.-C. (2016). Design, synthesis, and evaluation of cell permeable probes for protein kinases. *Tetrahedron* **72**, 58-68. doi:10.1016/j.tet.2015.10.053
Huai, J., Firat, E., Nil, A., Million, D., Gaedicke, S., Kanzler, B., Freudenberg, M., van Endert, P., Kohler, G., Pahl, H. L. et al. (2008). Activation of cellular death programs associated with immunosenescence-like phenotype in TPPII knockout mice. *Proc. Natl. Acad. Sci. USA* **105**, 5177-5182. doi:10.1073/pnas.0801413105
James, E. L., Michalek, R. D., Pitiyage, G. N., de Castro, A. M., Vignola, K. S., Jones, J., Mohney, R. P., Karoly, E. D., Prime, S. S. and Parkinson, E. K. (2015). Senescent human fibroblasts show increased glycolysis and redox homeostasis with extracellular metabolomes that overlap with those of irreparable DNA damage, aging, and disease. *J. Proteome Res.* **14**, 1854-1871. doi:10.1021/pr501221g
Kaushik, S. and Cuervo, A. M. (2015). Proteostasis and aging. *Nature Med.* **21**, 1406-1415. doi:10.1038/nm.4001
Kenzelmann Broz, D., Spano Mello, S., Bieging, K. T., Jiang, D., Dusek, R. L., Brady, C. A., Sidow, A. and Attardi, L. D. (2013). Global genomic profiling reveals an extensive p53-regulated autophagy program contributing to key p53 responses. *Genes Dev.* **27**, 1016-1031. doi:10.1101/gad.212282.112
Kruithof, E. K. O., Vassalli, J.-D., Schleuning, W.-D., Mattaliano, R. J. and Bachmann, F. (1986). Purification and characterization of a plasminogen activator inhibitor from the histiocytic lymphoma cell line U-937. *J. Biol. Chem.* **261**, 11207-11213. doi:10.1016/S0021-9258(18)67369-7
Kuilman, T. and Peeper, D. S. (2009). Senescence-messaging secretome: SMS-ing cellular stress. *Nat. Rev. Cancer* **9**, 81-94. doi:10.1038/nrc2560
Kuilman, T., Michaloglou, C., Vredeveld, L. C. W., Douma, S., van Doorn, R., Desmet, C. J., Aarden, L. A., Mooi, W. J. and Peeper, D. S. (2008). Oncogene-induced senescence relayed by an interleukin-dependent inflammatory network. *Cell* **133**, 1019-1031. doi:10.1016/j.cell.2008.03.039
Kumar, S., Millis, A. J. T. and Baglioni, C. (1992). Expression of interleukin 1-inducible genes and production of interleukin 1 by aging human fibroblasts. *Proc. Natl. Acad. Sci. USA* **89**, 4683-4687. doi:10.1073/pnas.89.10.4683
Kuo, C.-C., Chu, C.-Y., Lin, J.-J. and Lo, L.-C. (2010). Selective activation of SHP2 activity by cisplatin revealed by a novel chemical probe-based assay. *Biochem. Biophys. Res. Commun.* **391**, 230-234. doi:10.1016/j.bbrc.2009.11.037
Kurz, D. J., Decary, S., Hong, Y. and Erusalimsky, J. D. (2000). Senescence-associated β-galactosidase reflects an increase in lysosomal mass during replicative ageing of human endothelial cells. *J. Cell Sci.* **113**, 3613-3622. doi:10.1242/jcs.113.20.3613
Lee, B. Y., Han, J. A., Im, J. S., Morrone, A., Johung, K., Goodwin, E. C., Kleijer, W. J., DiMaio, D. and Hwang, E. S. (2006). Senescence-associated β-galactosidase is lysosomal β-galactosidase. *Aging Cell* **5**, 187-195. doi:10.1111/j.1474-9726.2006.00199.x
Liao M.-S. (2009). Development of activity probes based on benzyl fluorophosphonate. Master Thesis, National Taiwan University, Taiwan.
Lin, L., Sohar, I., Lackland, H. and Lobel, P. (2001). The human CLN2 protein/tripeptidyl-peptidase I is a serine protease that autoactivates at acidic pH. *J. Biol. Chem.* **276**, 2249-2255. doi:10.1074/jbc.M008562200
Lipetz, J. and Cristofalo, V. J. (1972). Ultrastructural changes accompanying the aging of human diploid cells in culture. *J. Ultrastruct. Res.* **39**, 43-56. doi:10.1016/S0022-5320(72)80005-4
Lu, W., Zhang, Y., McDonald, D. O., Jing, H., Carroll, B., Robertson, N., Zhang, Q., Griffin, H., Sanderson, S., Lakey, J. H. et al. (2014). Dual proteolytic pathways govern glycolysis and immune competence. *Cell* **159**, 1578-1590. doi:10.1016/j.cell.2014.12.001
Micsenyi, M. C., Sikora, J., Stephney, G., Dobrenis, K. and Walkley, S. U. (2013). Lysosomal membrane permeability stimulates protein aggregate formation in neurons of a lysosomal disease. *J. Neurosci.* **33**, 10815-10827. doi:10.1523/JNEUROSCI.0987-13.2013
Narita, M., Nuñez, S., Heard, E., Narita, M., Lin, A. W., Hearn, S. A., Spector, D. L., Hannon, G. J. and Lowe, S. W. (2003). Rb-mediated heterochromatin formation and silencing of E2F target genes during cellular senescence. *Cell* **113**, 703-716. doi:10.1016/S0092-8674(03)00401-X
Perez-Riverol, Y., Bai, J., Bandla, C., Hewapathirana, S., García-Seisdedos, D., Kamatchinathan, S., Kundu, D., Prakash, A., Frericks-Zipper, A., Eisenacher, M., et al. (2022). The PRIDE database resources in 2022: A Hub for mass spectrometry-based proteomics evidences. *Nucleic Acids Res.* **50**, D543-D552. doi:10.1093/nar/gkab1038
Robbins, E., Levine, E. M. and Eagle, H. (1970). Morphologic changes accompanying senescence of cultured human diploid cells. *J. Exp. Med.* **131**, 1211-1222. doi:10.1084/jem.131.6.1211
Rockel, B., Kopec, K. O., Lupas, A. N. and Baumeister, W. (2012). Structure and function of tripeptidyl peptidase II, a giant cytosolic protease. *Biochim. Biophys. Acta* **1824**, 237-245. doi:10.1016/j.bbapap.2011.07.002
Salama, R., Sadaie, M., Hoare, M. and Narita, M. (2014). Cellular senescence and its effector programs. *Genes Dev.* **28**, 99-114. doi:10.1101/gad.235184.113
Sardiello, M., Palmieri, M., di Ronza, A., Medina, D. L., Valenza, M., Gennarino, V. A., Di Malta, C., Donaudy, F., Embrione, V., Polishchuk, R. S. et al. (2009). A gene network regulating lysosomal biogenesis and function. *Science* **325**, 473-477. doi:10.1126/science.1174447
Schroder, W. A., Le, T. T. T., Major, L., Street, S., Gardner, J., Lambley, E., Markey, K., MacDonald, K. P., Fish, R. J., Thomas, R. et al. (2010). *A* physiological function of inflammation-associated SerpinB2 is regulation of adaptive immunity. *J. Immunol.* **184**, 2663-2670. doi:10.4049/jimmunol.0902187
Serrano, M., Lin, A. W., McCurrach, M. E., Beach, D. and Lowe, S. W. (1997). Oncogene *ras* provokes premature cell senescence associated with accumulation of p53 and $p16^{INK4a}$. *Cell* **88**, 593-602. doi:10.1016/S0092-8674(00)81902-9
Sharpless, N. E. and Sherr, C. J. (2015). Forging a signature of *in vivo* senescence. *Nat. Rev. Cancer* **15**, 397-408. doi:10.1038/nrc3960
Sherr, C. J. and DePinho, R. A. (2000). Cellular senescence: Mitotic clock or culture shock? *Cell* **102**, 407-410. doi:10.1016/S0092-8674(00)00046-5
Sieber, S. A., Mondala, T. S., Head, S. R. and Cravatt, B. F. (2004). Microarray platform for profiling enzyme activities in complex peoteomes. *J. Am. Chem. Soc.* **126**, 15640-15641. doi:10.1021/ja044286+
Stepensky, P., Rensing-Ehl, A., Gather, R., Revel-Vilk, S., Fischer, U., Nabhani, S., Beier, F., Brummendorf, T. H., Fuchs, S., Zenke, S. et al. (2014). Early-onset Evans syndrome, immunodeficiency, and premature immunosenescence associated with tripeptidyl-peptidase II deficiency. *Blood* **125**, 753-761. doi:10.1182/blood-2014-08-593202
Succoio, M., Comegna, M., D'Ambrosio, C., Scaloni, A., Filiberto Cimino, F. and Faraonio, R. (2015). Proteomic analysis reveals novel common genes modulated in both replicative and stress-induced senescence. *J. Proteomics* **128**, 18-29. doi:10.1016/j.jprot.2015.07.010
Thorsen, S., Philips, M., Selmer, J., Lecander, I. and Astedt, B. (1988). Kinetics of inhibition of tissue-type and urokinase-type plasminogen activator by plasminogen-activator inhibitor type 1 and type 2. *Eur. J. Biochem.* **175**, 33-39. doi:10.1111/j.1432-1033.1988.tb14162.x
Tomkinson, B. (1999). Tripeptidyl peptidases: enzymes that count. *Trends Biochem. Sci.* **24**, 355-359. doi:10.1016/S0968-0004(99)01435-8
Vidal-Donet, J. M., Cárcel-Trullols, J., Casanova, B., Aguado, C. and Knecht, E. (2013). Alterations in ROS activity and lysosomal pH account for distinct patterns of macroautophagy in LINCL and JNCL fibroblasts. *PLoS ONE* **8**, e55526. doi:10.1371/journal.pone.0055526
Wei, W. and Sedivy, J. M. (1999). Differentiation between senescence (M1) and crisis (M2) in human fibroblast cultures. *Exp. Cell Res.* **253**, 519-522. doi:10.1006/excr.1999.4665
West, M. D., Shay, J. W., Wright, W. E. and Linskens, M. H. K. (1996). Altered expression of plasminogen activator and plasminogen activator inhibitor during cellular senescence. *Exp. Gerontol.* **31**, 175-193. doi:10.1016/0531-5565(95)02013-6
Zhang, H., Pan, K.-H. and Cohen, S. N. (2003). Senescence-specific gene expression fingerprints reveal cell-type-dependent physical clustering of up-regulated chromosomal loci. *Proc. Natl. Acad. Sci. USA* **100**, 3251-3256. doi:10.1073/pnas.2627983100
Zhang, S.-J., Zou, M., Lu, L., Lau, D., Ditzel, D. A. W., Delucinge-Vivier, C., Aso, Y., Descombes, P. and Bading, H. (2009). Nuclear calcium signaling controls expression of a large gene pool: identification of a gene program for acquired neuroprotection induced by synaptic activity. *PLoS Genet.* **5**, e1000604. doi:10.1371/journal.pgen.1000604
Zhang, C., Ponugoti, B., Tian, C., Xu, F., Tarapore, R., Batres, A., Alsadun, S., Lim, J., Dong, G. and Graves, D. T. (2015). FOXO1 differentially regulates both normal and diabetic wound healing. *J. Cell Biol.* **209**, 289-303. doi:10.1083/jcb.201409032

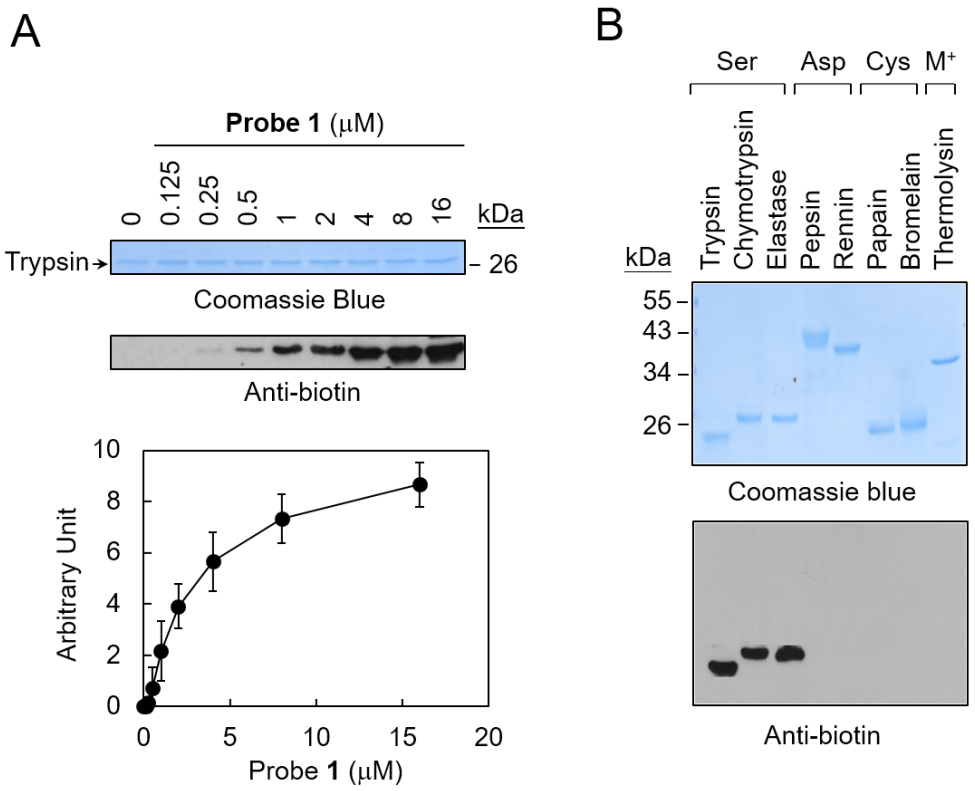

Fig. S1. Labeling property of probe **1**. **(A)** In parallel experiments, one μg each of trypsin was incubated with indicated amounts of probe **1** at 25ºC for 10 mins and separated on a 10% SDS-polyacrylamide gel. One gel was stained with Coomassie blue and the other was subjected to immunoblotting analysis using anti-biotin antibody. Quantification of the labeled proteins were plotted (bottom panels). The values were obtained from the average of three independent experiments. Error bars represent standard deviation (SD). **(B)** One μg each of the indicated proteases was labeled with probe **1** (3 μM) at 25ºC for 10 min. The labeled proteins were separated on a 10% SDS-polyacrylamide gel and then stained with Coomassie blue (top panel) followed by immunoblotting analysis using anti-biotin antibody (bottom panel).

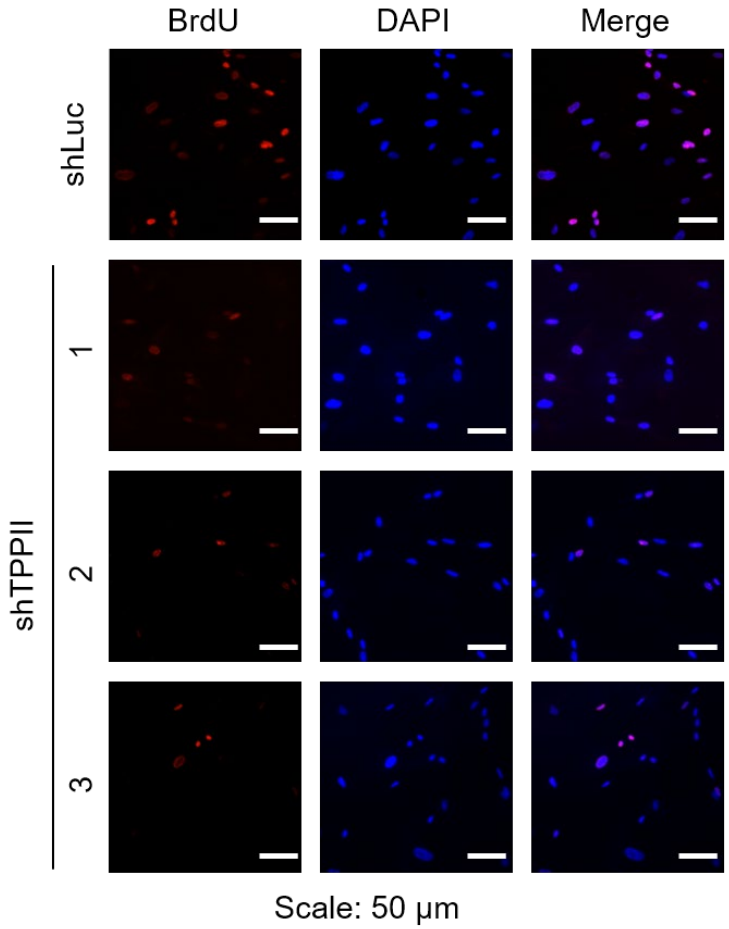

Fig. S2. IMR90 cells were infected with lentivirus carrying TPPII- or Luciferase-targeting shRNA sequences. Three days after infection, cells were re-seeded on cover slide. One day later, cells were incubated with 40 μM BrdU for 16 h, fixed, and then stained with anti-BrdU antibody (red) and DAPI (blue). The scale bar represents 50 μm.

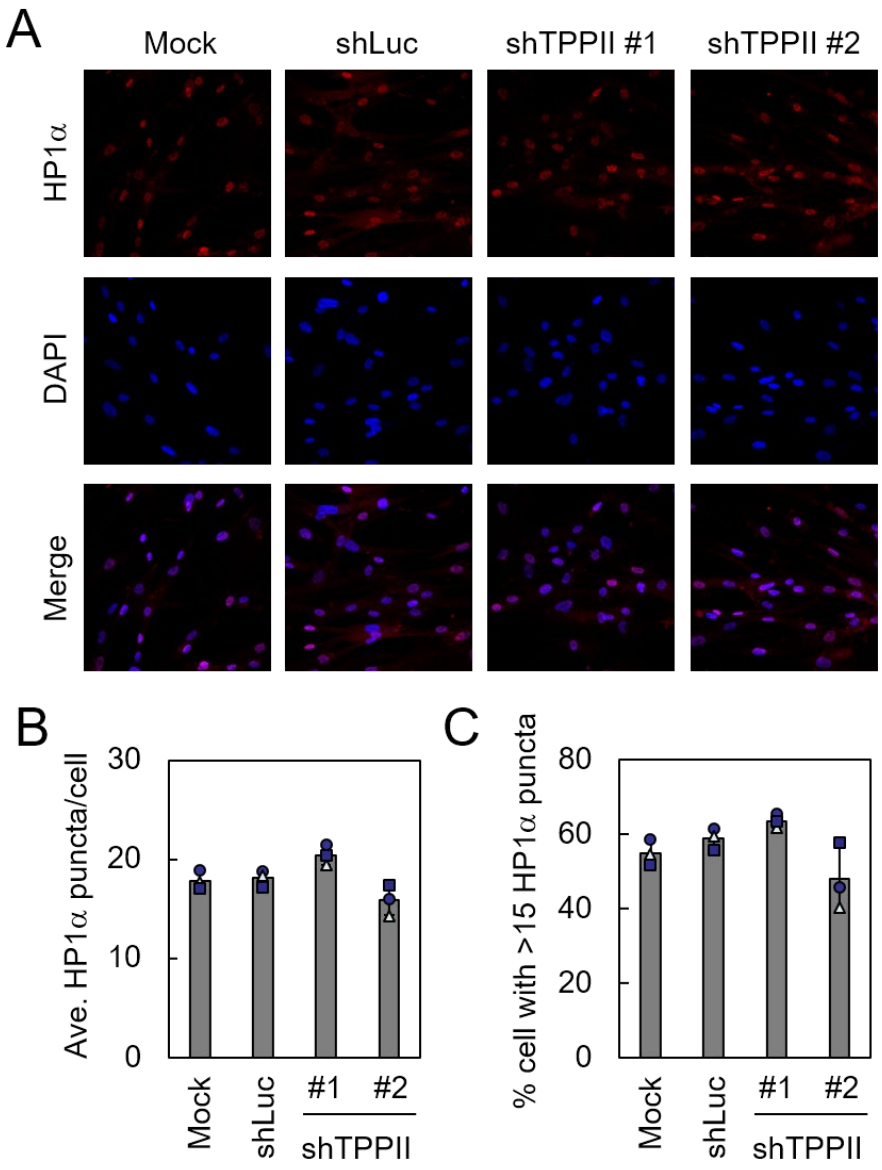

Fig. S3. IMR90 cells were infected with lentivirus carrying TPPII- or Luciferase-targeting shRNA sequences. (A) Three days after infection, cells were re-seeded on cover slide, fixed, and then stained with anti-HP1α antibody (red) and DAPI (blue). The average numbers of HP1α puncta per cell and the percentage of cells with >15 puncta were quantified in (B) and (C), respectively. Quantification results in (B, C) were conducted from the average of 3 independent experiments.

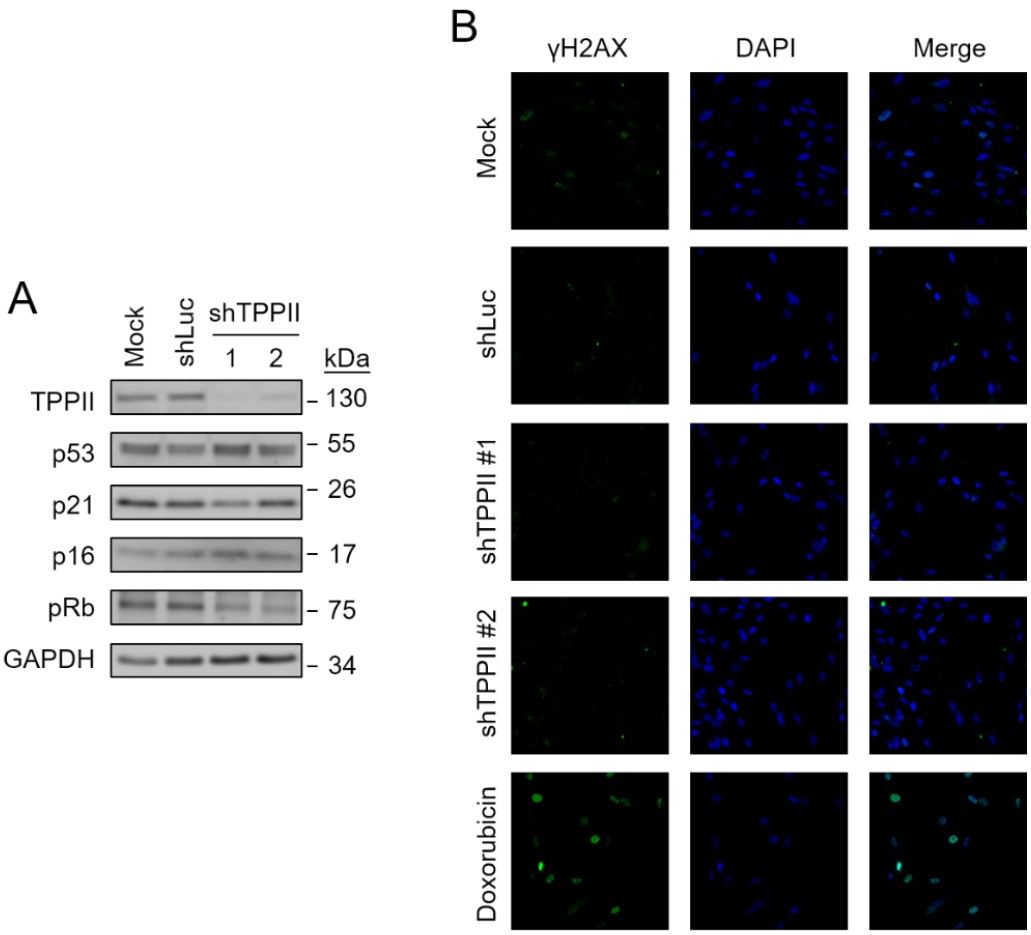

Fig. S4. IMR90 cells were infected with lentivirus carrying TPPII- or Luciferase-targeting shRNA sequences. (A) Cell extracts were prepared four days after infection and then analyzed by immunoblots using the indicated antibodies. (B) Immunofluorescence assays were also performed using anti-γH2AX antibody (green). The cell nuclei were stained with DAPI (blue).

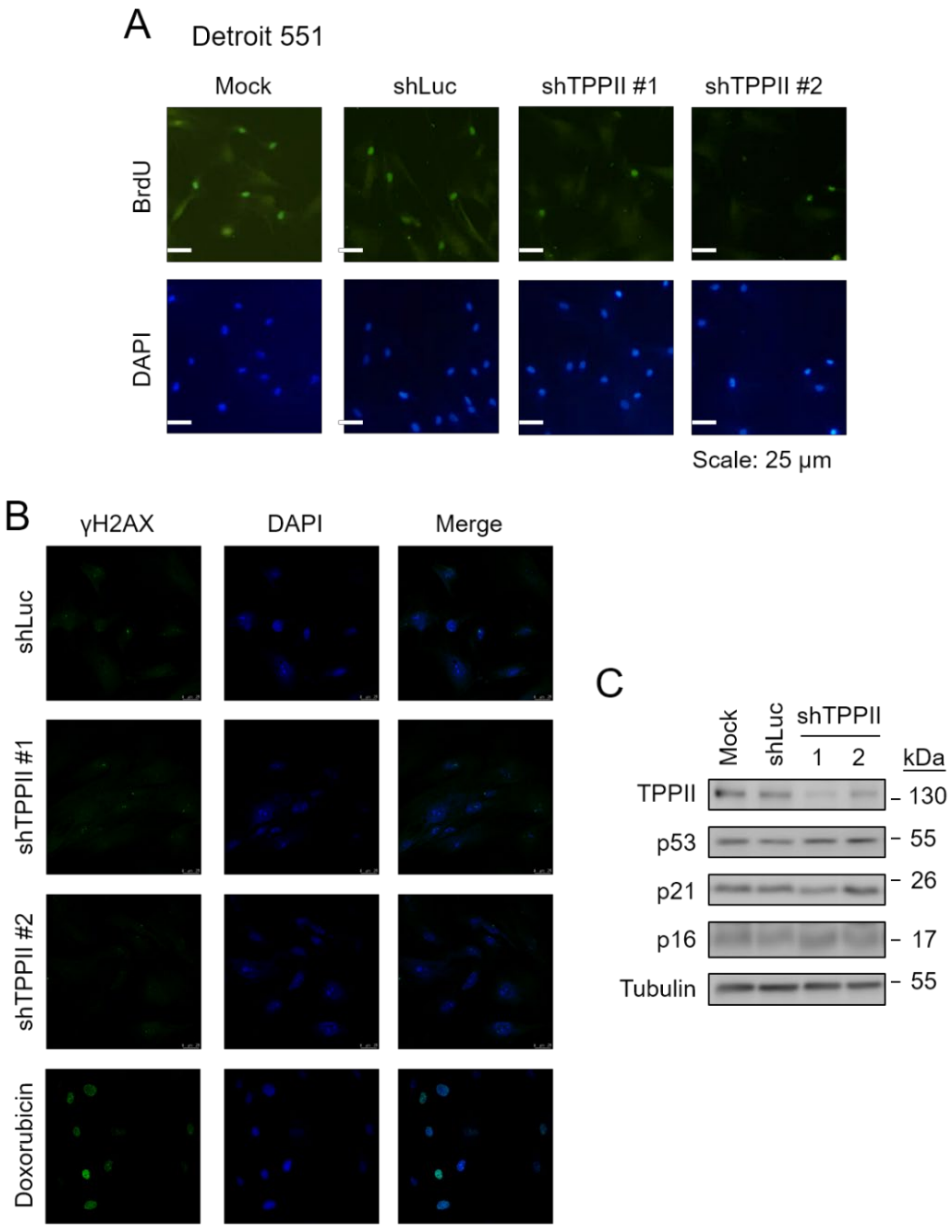

Fig. S5. Detroit551 cells were infected with lentivirus carrying TPPII- or Luciferase-targeting shRNA sequences. (A) Cells were incubated with 40μM BrdU for 16 h, fixed, and then stained with anti-BrdU antibody (green) and DAPI (blue). (B) In another experiment, cells were immunostained with anti-γH2AX antibody. (C) Cell extracts were prepared four days after infection and then analyzed by immunoblots using the indicated antibodies.

Table S1. Serine hydrolases with altered activities in senescence.

Gene	Protein Name	Ratio[1)]
Increased in senescent cells		
ACOT2	Acyl-coenzyme A thioesterase 2	100
PREP	Prolyl endopeptidase	100
LYPLA2	Lysophospholipase II/Acyl-protein thioesterase 2	17.14
ABHD14B	Abhydrolase domain-containing protein 14B	1.98
TPP1	Tripeptidyl-peptidase 1	1.92
ABHD12	Abhydrolase domain-containing 12/Monoacylglycerol lipase	1.79
LACTB	Lactamase Beta/Serine beta-lactamase-like protein LACTB	1.47
SIAE	Sialate O-acetylesterase	1.27
Decreased in senescent cells		
FASN	Fatty acid synthase	0.80
TPP2	Tripeptidyl-peptidase 2	0.78
ACOT1	Acyl-coenzyme A thioesterase 1	0.76
PNPLA6	Patatin like phospholipase domain containing 6/Neuropathy target esterase	0.75
ABHD10	Abhydrolase domain containing 10	0.73
NCEH1	Neutral cholesterol ester hydrolase 1	0.73
PPME1	Protein phosphatase methylesterase 1	0.70
LYPLA1	Lysophospholipase 1/Acyl-protein thioesterase 1	0.58
MGLL	Monoglyceride lipase	0.55
PAFAH1B3	Platelet-activating factor acetylhydrolase 1b catalytic subunit 3	0.52
ESD	Esterase D/Formylglutathione hydrolase	0.50
PAFAH2	Platelet-activating factor acetylhydrolase 2	0.49
uPA	Urokinase-type plasminogen activator	0.01

[1)] Comparison of protein abundance by senescent/young cells; 100 and 0.01 represented the detection of proteins only in senescent and proliferating cells, respectively.